Chapter 4 Results and Discussion

This chapter presents the experiment results and discussions on CoPtCr-SiO_2 perpendicular recording media. This chapter includes the effects of different underlayers and effects of the depositing parameter on PMR properties.

Different substrates of perpendicular magnetic recording media usually turn out to have different magnetic performance. The films deposited on SiO_2 substrate were used to examine the texture from XRD result while the others on glass substrate were used to determine the magnetic properties. In order to obtain recording performance, Read-and-Write tests of the films deposited on textured-AlMg substrates were performed in the final section.

SiO_2 content

The innovation of the recording target we used is a collaboration with Heraeus Corporation with 10 % SiO_2 of $[CoPt_{20}Cr_{10}]_{90}$-$(SiO_2)_{90}$ media. Compared our composition with reported one [42], as indicated in Fig. 4.1, our SiO_2 content is approaching to the reported one with best magnetic performance around 11%. The perpendicular Hc is optimized at 11% SiO_2, and the ***Ku*** value would drop seriously while adding too much SiO_2 into the media. As a result, the SiO_2 content we picked up is quite promising to perform best magnetic properties.

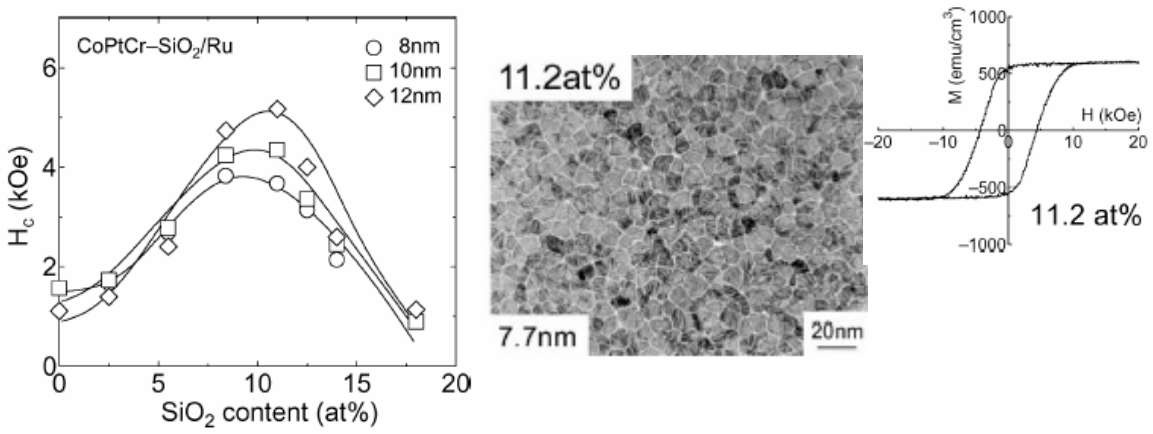

Figure 4.1 The magnetic performance of altering the SiO_2 content. [42]

4.1 Effects of Different Intermediate Layers on PMR

Intermediate layers deposited between recording layer and soft underlayer plays a vital role of promoting the texture of perpendicular recording media. It was apparently observed from the XRD result as shown in Fig. 4.2 that the perpendicular anisotropy was significantly degraded, resulting from poor alignment of the c-axis of the recording layer, while depositing a single recording layer on substrate at room temperature. Therefore, the most important issue is to find appropriate underlayer and seedlayer to enhance the film growth of the recording layer. In addition, the lattice constant of CoPtCr-SiO_2 could be calculated from the following equation (a=2.5871 Å and c=4.2077 Å).

$$\sin^2\theta = \frac{\lambda^2}{4}\left\{\frac{4}{3}\frac{(h^2+hk+k^2)}{a^2}+\frac{l^2}{c^2}\right\}$$

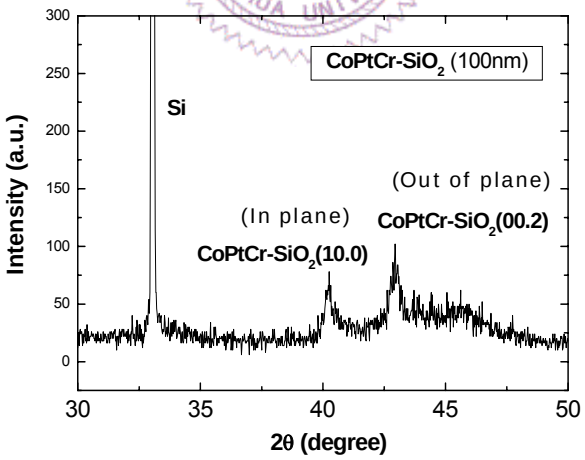

Figure 4.2 The XRD profile of CoPtCr-SiO_2 (100±5 nm).

This section would present the effects of intermediate layers on Pt/Ru/ CoPtCr-SiO_2 media by inserting a buffer-layer of Ta or Tb beneath this media. The performance of each media will be given first, and the

comparison between these media would be discussed later.

4.1.1 Pt/Ru/CoPtCr-SiO_2 Media

In general, microstructure of thin film is strongly dependent on the parameters of deposition such as thickness variation, working pressure, and substrate bias and so on. In addition, magnetic properties of magnetic film also significantly relate to the microstructure. The influence of important parameter would be investigated in the following discussion.

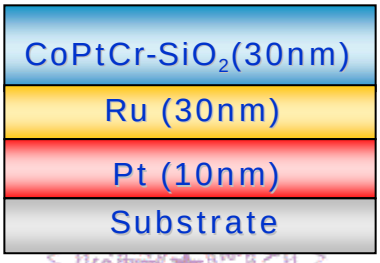

Figure 4.3 Film structure of PRM.

4.1.1.1 Effect of CoPtCr-SiO_2 Recording Layer Thickness

Thickness reduction is an important concern of recording performance. For example, writing flux could completely go back to head with a close loop without any loss. Furthermore, increasing the thickness of recording layer would result in larger magnetic clusters, and thus in high media noise.

Many studies had mentioned the influence of the recording layer thickness, which reported that there was a trade-off between thermal stability and SNR performance as increasing thickness of CoPtCr-SiO_2, as described in Fig. 4.4[29] and Fig. 4.5[36].The optimal thickness was

about 8-12 nm; therefore, we should drive the thickness approaching to this optimal value.

The texture of CoPtCr-SiO_2 (00.2) and anisotropy orientation were improved while depositing 30 nm CoPtCr-SiO_2 recording layer as shown in Fig. 4.6 and Fig. 4.7, which resulted from proper grain growth. On the contrary, the magnetic properties were declined due to increased intergranular exchange coupling while the thickness of recording layer was larger than 35nm.

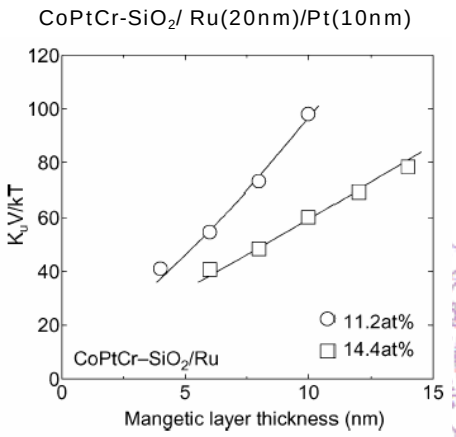

Figure 4.4 The dependence on magnetic layer thickness. [29]

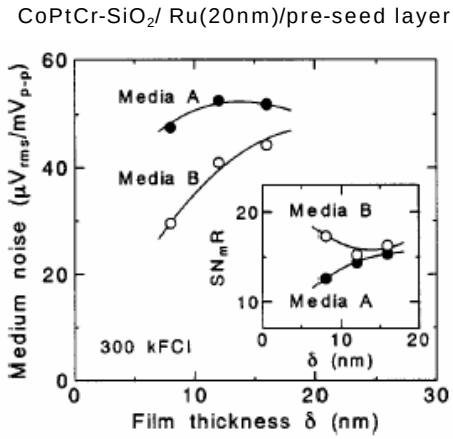

Figure 4.5 Media noise dependent on magnetic layer thickness. [36]

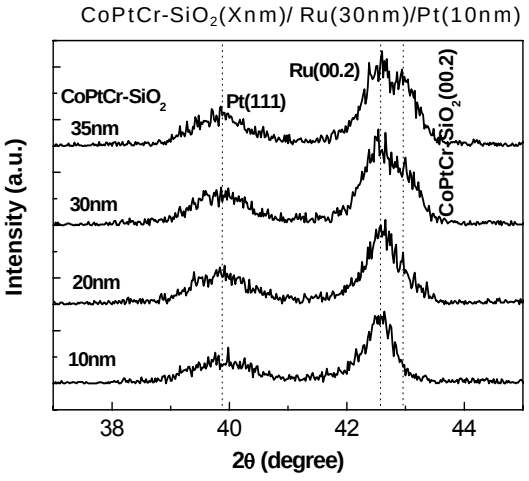

Figure 4.6 XRD profiles of various thickness of recording layer.

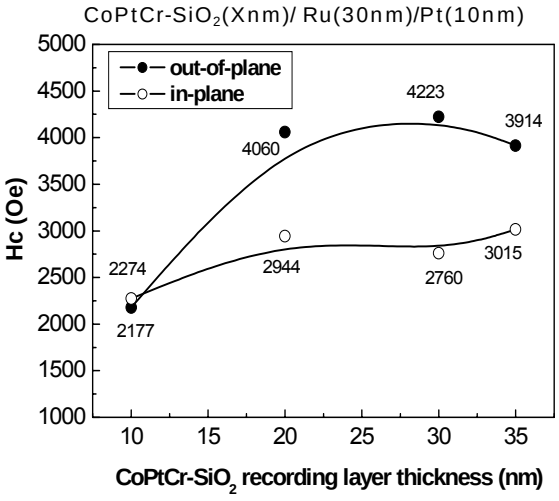

Figure 4.7 VSM result of various thickness of recording layer.

4.1.1.2 Effect of Working Pressure of CoPtCr-SiO_2 Recording Layer

The texture of recording layer was strongly dependent on the working pressure of CoPtCr-SiO_2 as shown in Fig. 4.8. The peak of c-axis (00.2) got closer to the peak of Ru (00.2) while increasing the working pressure of CoPtCr-SiO_2, especially at 25 mTorr; that is, high degree of lattice match along c-axis occurred between CoPtCr-SiO_2 layer and Ru layer. In addition, the magnetic property of anisotropy orientation ($H_{C\ out\text{-}of\text{-}plane}/H_{C\ in\text{-}plane}$) as described in Fig. 4.9 was highly improved at 25 mTorr as well as the large perpendicular coercivity.

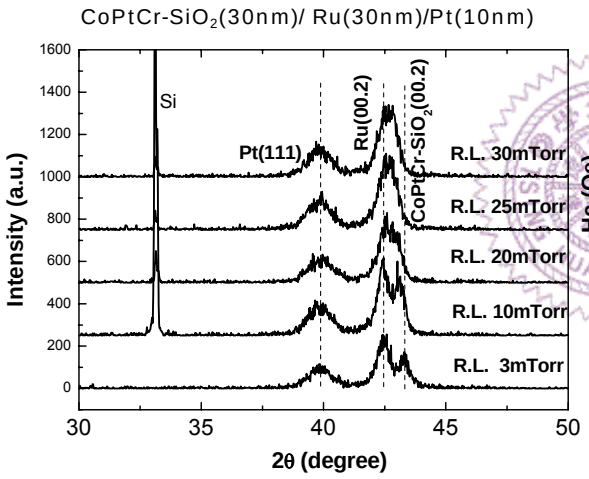

Figure 4.8 XRD profiles of working pressure effect on recording layer.

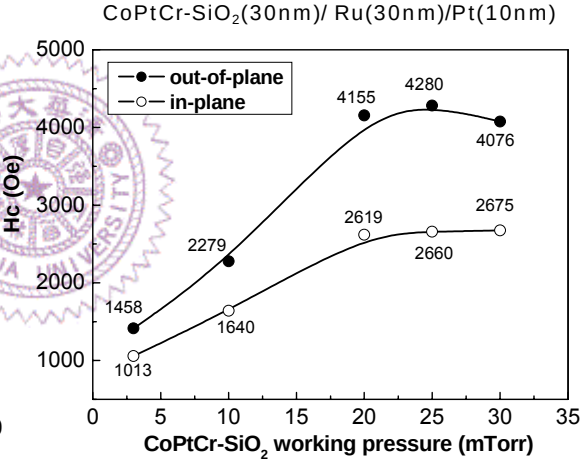

Figure 4.9 VSM result of working pressure effect on recording layer.

4.1.1.3 Effect of Ru seedlayer thickness

Introducing proper underlayers deposited below recording layer would not only get high degree lattice match, but enhance the perpendicular anisotropy and the microstructure of recording layer. The texture and

perpendicular Hc were enhanced as the thickness of Ru seedlayer were thick enough to promote epitaxial growth along c-axis.

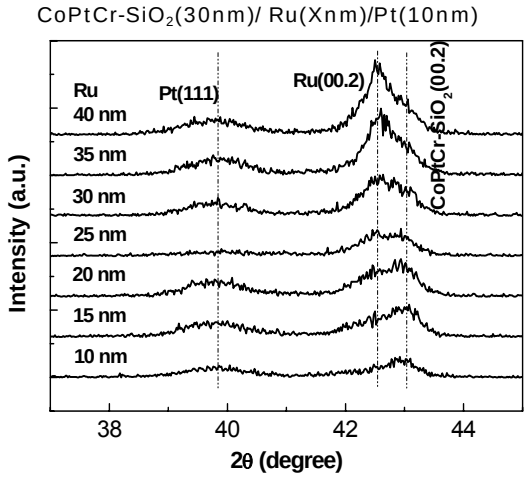

Figure 4.10 XRD profile of thickness variation of Ru seedlayer.

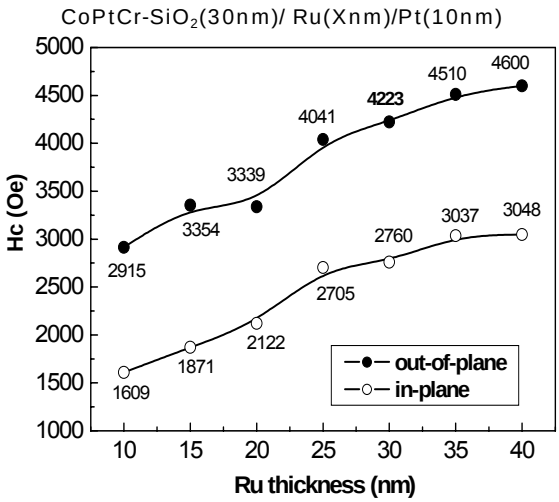

Figure 4.11 VSM result of thickness variation of Ru seedlayer.

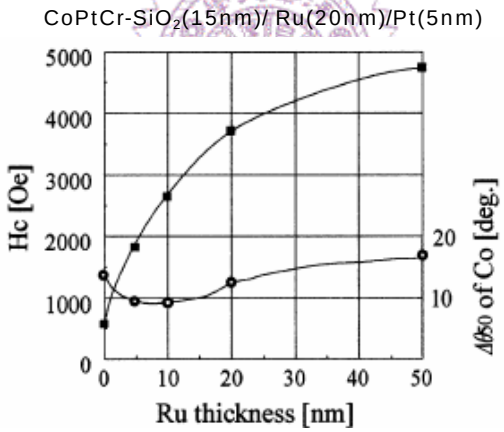

Figure 4.12 Dependence of perpendicular Hc on Ru underlayer thickness. [43]

As a consequence, the thickness had to be larger than 30nm that the peak intensity and anisotropy orientation could be enhanced, as shown in Fig. 4.10 and Fig. 4.11. The thickness larger than 35nm, however, would deteriorate the texture of recording and increase the in-plan coercivity. This trend was similar to the reference paper [43] as illustrated in Fig. 4.12.

4.1.1.4 Effect of Pt underlayer thickness

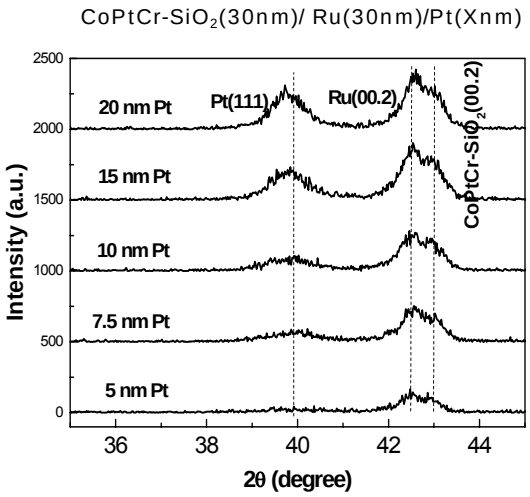

Figure 4.13 XRD profile of thickness variation of Pt underlayer.

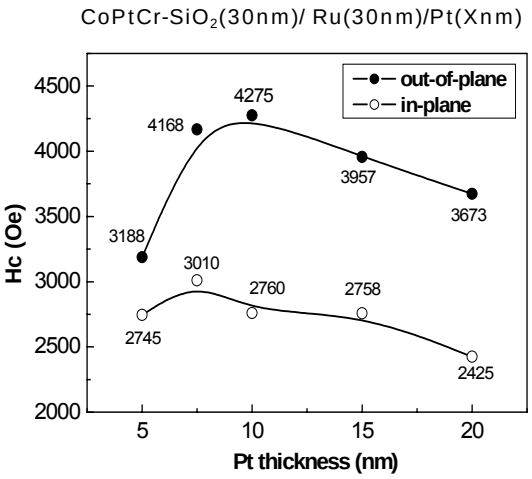

Figure 4.14 VSM result of thickness variation of Pt underlayer.

In order to make the film growth of perpendicular recording perfect on f.c.c.-substrate, the Pt underlayer with f.c.c. structure was introduced for improving epitaxial growth, as shown in Fig. 4.13. In addition, as indicated in Fig. 4.14, enhanced anisotropy orientation of magnetic properties was attained while depositing Pt underlayer with the thickness larger 10nm.

4.1.1.5 Ultra-Clean Sputter Process

The magnetic properties of the films were about the same while depositing at background pressure around $8*10^{-8}$~$8*10^{-7}$ Torr, as seen in Fig. 4.15. However, the film deposited at $4*10^{-8}$ Torr had better magnetic performance such as higher perpendicular coercivity (Hc> 4.5 kOe) and unity squareness. It represented that the ultra-clean sputter process was in great demand in achieving ultra-high recording density perpendicular

recording media.

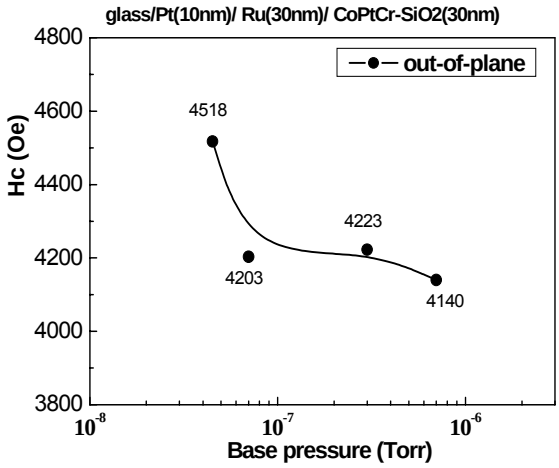

Figure 4.15 Magnetic Performance comparisons with different vacuum.

4.1.2 Ta/Pt/Ru/CoPtCr-SiO_2 Media

The texture of c-axis (00.2) and anisotropy orientation of Pt/Ru/CoPtCr -SiO_2 media were not optimized due to imperfect epitaxal growth of Pt underlayer and Ru seedlayer. Therefore, the thin Ta buffer-layer deposited under Pt underlayer was introduced to improve the texture of Pt underlayer, Ru seedlayer and further recording layer. The structure of the film and the deposition parameters were described in Fig. 4.16.

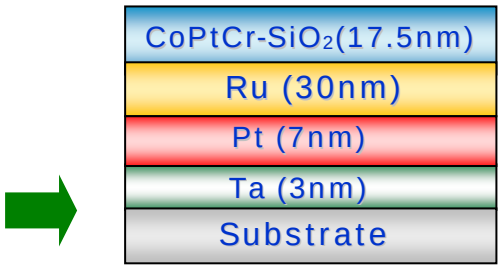

Figure 4.16 Inserting Ta buffer-layer into perpendicular recording media.

The study [43] mentioned that by introducing Ta pre-coat layer,

Ta/Ru/CoPtCr-SiO_2 media would effective improve roughness, grain size, crystal orientation, and perpendicular Hc. As indicated in Fig. 4.17, each magnetic property was superior to the Pt/Ru/CoPtCr-SiO_2 media. As a consequence, we could improve all the performance by the insertion of Ta layer.

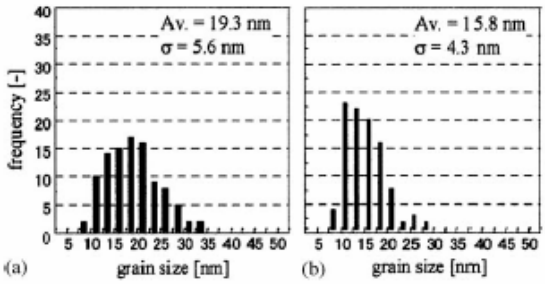

(a)CoPtCr-SiO_2(15nm)/ Ru(10nm)/Pt(2nm) (b)CoPtCr-SiO_2(15nm)/ Ru(10nm)/Ta(2nm)

Figure 4.17 AFM images and grain size distribution of these two media. [43]

4.1.2.1 Effect of Ta Buffer-layer Thickness

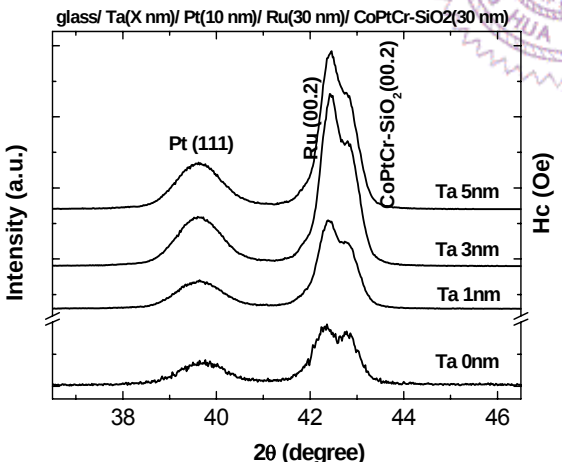

Figure 4.18 XRD profile of thickness variation of Ta buffer-layer.

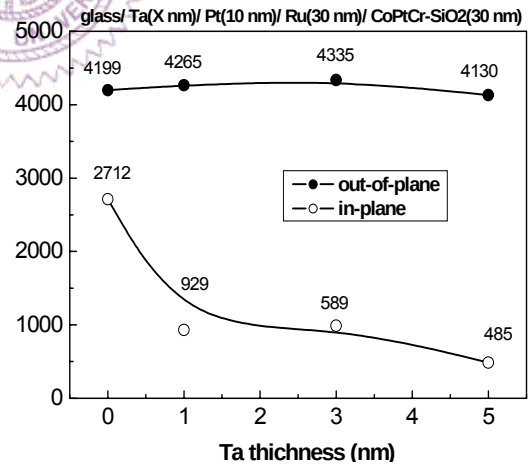

Figure 4.19 VSM result of thickness variation of Ta buffer-layer.

Fig. 4.18 sketched that texture of each layer was greatly enhanced by inserting the Ta buffer-layer. In addition, the anisotropy orientation as revealed in Fig. 4.19 was also improved as the decreasing in-plane Hc.

Furthermore, the magnetic properties were promoted such as squreness around 1 and higher negative Hn. No doubt that Ta buffer-layer was a good choice for solving all the problems on our study.

4.1.2.2 Effect of CoPtCr-SiO_2 recording layer Thickness

The thickness of CoPtCr-SiO_2 recording layer was expected to be reduced in order to diminish the distance between SPT head and soft underlayer and subsequently ensured that all magnetic flux could pass through recording layer and soft underlayer without loss. In addition, the media noise would be reduced due to reduced magnetic cluster size as decreasing the thickness of recording layer.

As observed in Fig. 4.20, the thickness of recording layer could be further reduced to 20nm and achieve even better magnetic property, i.e. perpendicular Hc about 4.3 kOe, as seen in Fig. 4.21. It was because that Ta buffer-layer played a decisive role at improving both the texture of c-axis and anisotropy orientation.

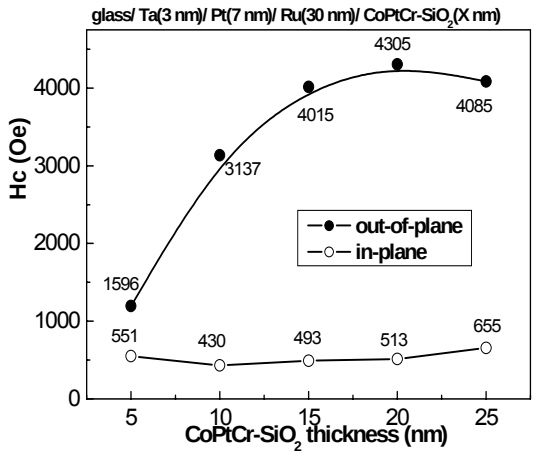

Figure 4.20 VSM result of thickness variation of CoPtCr-SiO_2 recording.

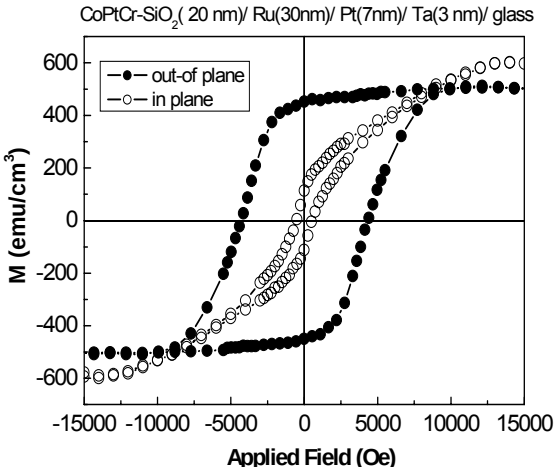

Figure 4.21 M-H loop of Ta(3nm) /Pt(7nm)/Ru(30nm)/CoPtCr-SiO_2(20nm).

Furthermore, texture-AlMg substrate was used instead of glass to examine the thickness dependent on recording layer. As shown in Fig 4.22, the optimal thickness of recording layer was further reduced to 17.5 nm with better perpendicular Hc about 4.6 kOe. Moreover, the SQ value of the media was almost 1 as optimal thickness was attained.

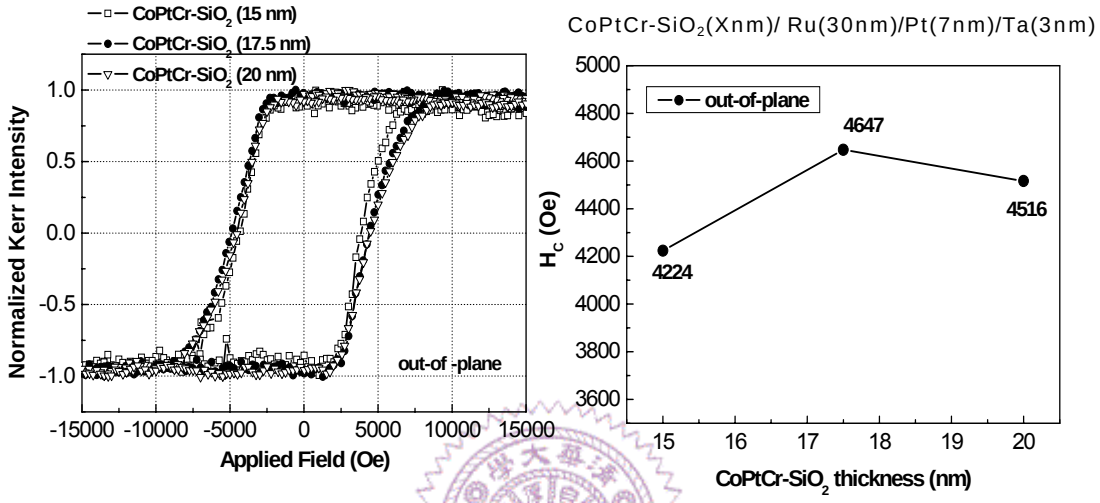

Figure 4.22 Magnetic property of Ta(3nm)/Pt(7nm)/Ru(30nm)/CoPtCr-SiO_2(Xnm).

4.1.2.3 Substrate Effect on PMR

Since the recording performance of the films would be examined through R&W test, it had to transfer form glass substrate to commercial substrate for R&W test such as AlMg substrate. Textured-AlMg substrate is textured by laser and is precisely controlled in order to perform the "Zone-Texture", which provides smooth surface of data zone and prevents the contact of head with media at contact-start-stop, CSS Zone.

As illustrated in Fig. 4.23 and Fig. 4.24, these films deposited on different substrates showed the same superior performance as on glass substrate. It also interpreted that our optimal film structure was the best

option for ultra-high recording density perpendicular media. In addition, textured-AlMg was the best option for R&W test due to its superior magnetic properties.

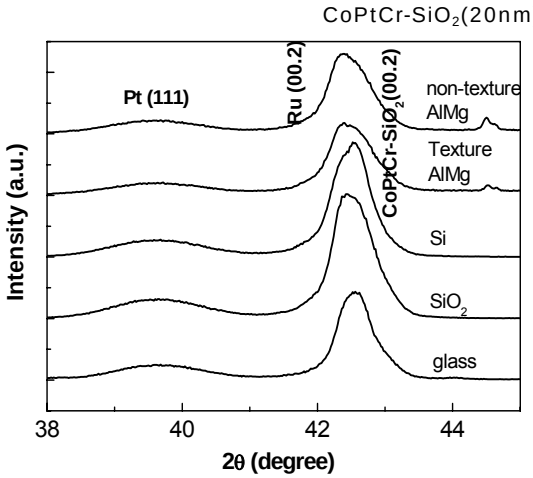

Figure 4.23 XRD profiles of these films deposited on different substrates.

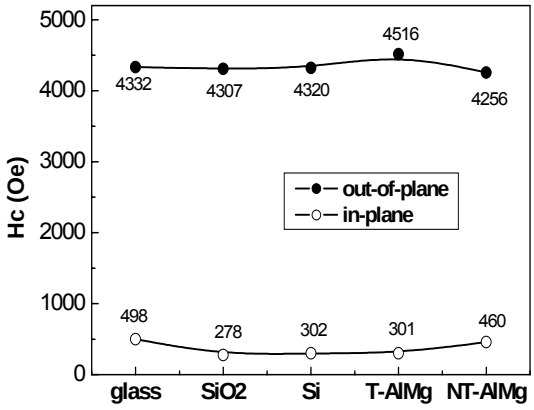

Figure 4.24 VSM results of these films deposited on different substrates.

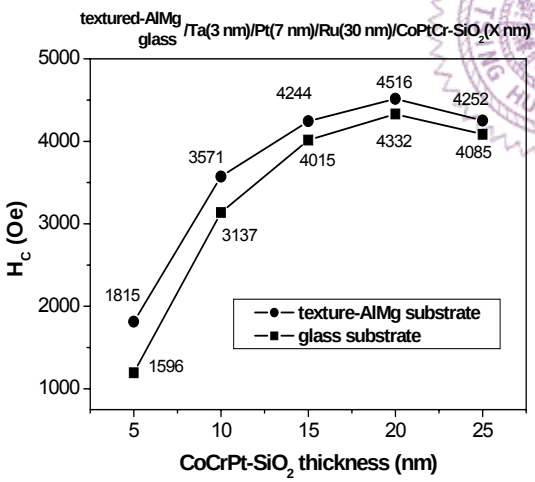

Figure 4.25 VSM results of these two films deposited on glass and textured-AlMg substrate.

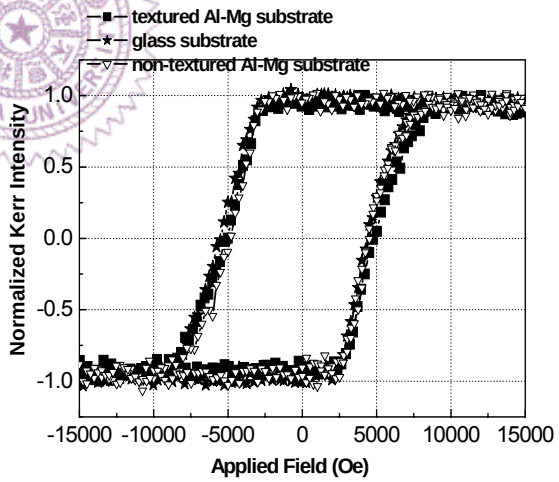

Figure 4.26 Magnetic properties of the films deposited on glass and AlMg substrates by PMOKE.

Furthermore, the previous piles work on parameter study had to be reconfirmed on different substrates. Subsequently, the thickness dependence on different substrates had been investigated in Fig. 4.25 and Fig. 4.26. It was very obviously to recognize that the trend of the film on

glass substrate and the one on textured-AlMg substrate were much similar to each other. Moreover, the magnetic properties of textured-AlMg substrate also presented excellent perpendicular Hc and almost unity SQ.

4.1.3 Tb/Pt/Ru/CoPtCr-SiO_2 Media

In order to achieve high recording density beyond 100 Gbits/in^2 of perpendicular magnetic recording media, enhancement of grain isolation is vital issue to obtain high SNR (signal-to-noise ratio). On the other hand, perpendicular Hc and SQ value have also to be optimized for resisting thermal fluctuation. However, there still exist many challenges of CoPtCr-SiO_2 granular magnetic system, such as non-uniform grain size distribution and the indistinct segregation mechanism of SiO_2. We would like introduce this new Tb underlayer of CoPtCr-SiO_2 media for both enhancement of SiO_2 segregation at grain boundaries and refinement of grain size of the granular magnetic grains. Furthermore, good magnetic performance is accompanied by the improvement of Tb underlayer.

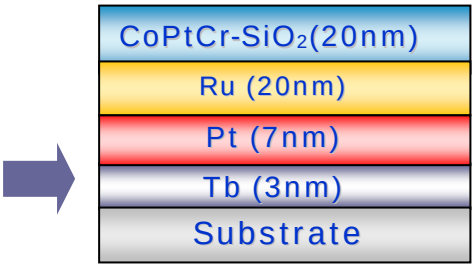

Figure 4.27 Inserting Tb buffer-layer into perpendicular recording media

4.1.4 Comparison of these three media

Since the insertion of buffer-layer affects performance of the whole

films a lot, the following would present several comparisons between these three media by magnetic performance and microstructure. In particular, stress effect is introduced to reveal the influence of different underlayers.

First, the magnetic performances were described in Fig. 4.28 and Fig 4.29. The media with Ta buffer-layer have highly reduced in-plane Hc to 413.23 Oe. However, it is obvious that the media with Tb buffer-layer has excellent anisotropy orientation, i.e. highest perpendicular Hc～4500 Oe and lowest in-plane Hc～195 Oe, which is superior to the two media with and without Ta buffer-layer. In consequence, the insertion of Tb buffer-layer indeed makes a large enhancement at magnetic performance by merely 3nm buffer-layer beneath previous Pt/Ru/CoPtCr-SiO_2 media.

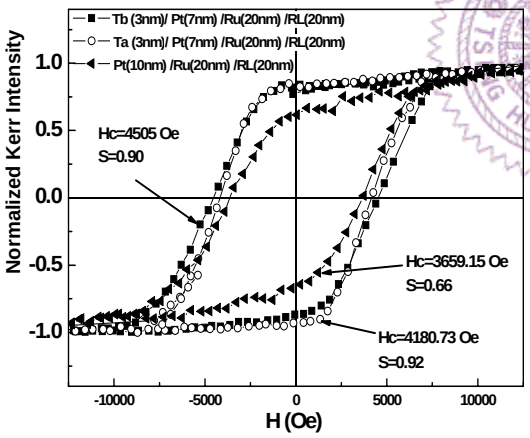

Figure 4.28 M-H loop of the media with different underlayers (perpendicular).

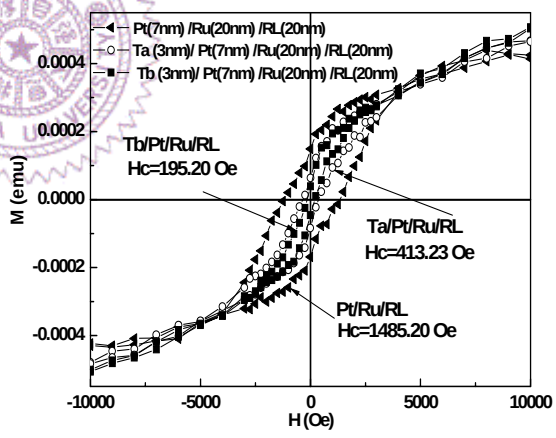

Figure 4.29 M-H loop of the media with different underlayers (in-plane).

From XRD profiles as shown in Fig. 4.30, the media with Tb buffer-layer apparently have strong peaks of CoPtCr-SiO_2 (00.2) and Pt (111) than the media without it. That is, the texture is highly promoted and it can be expected that better microstructure and magnetic performance

would be achieved.

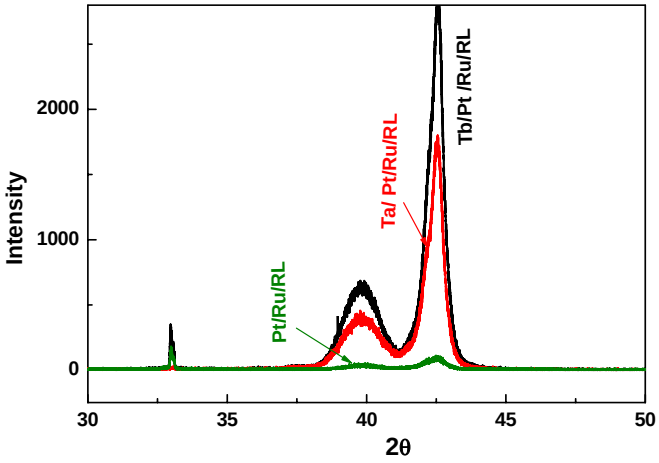

Figure 4.30 XRD profiles of the media with different underlayers.

In addition to the intensity of XRD, the c-axis distribution is much oriented as evidenced in Fig. 4.31. Although the media with Ta buffer-layer has narrowed the distribution to 5.693, the one with Tb buffer-layer can even promote to 4.515, which is highly textured compared than the one without Tb buffer-layer.

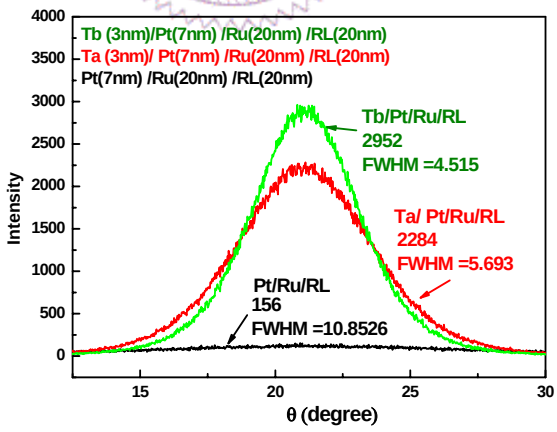

Figure 4.31 c-axis distribution of the media with different underlayers.

4.1.4.1 Stress examination of the media

To further understand the influence of Tb underlayer, the observation of stress effect was performed, as shown in Fig. 4.32 and Fig. 4.33. The

curvature measurement was performed on the films deposited on ultra-thin Si substrate (300um). The residual stress could be derived by using the Stoney's equation [25]. The media with Tb buffer-layer shows the largest tensile stress, which was reported to enhance perpendicular Hc [25].

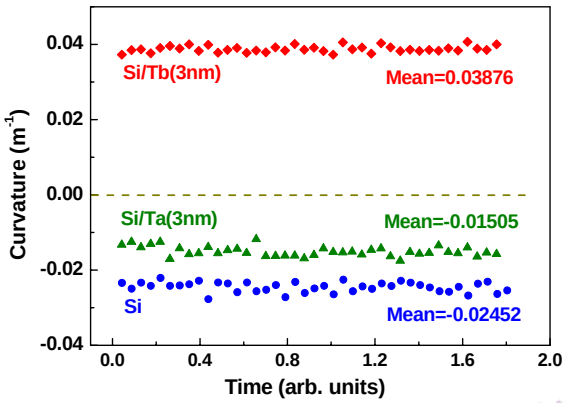

Figure 4.32 Curvature of single Tb and Ta layer.

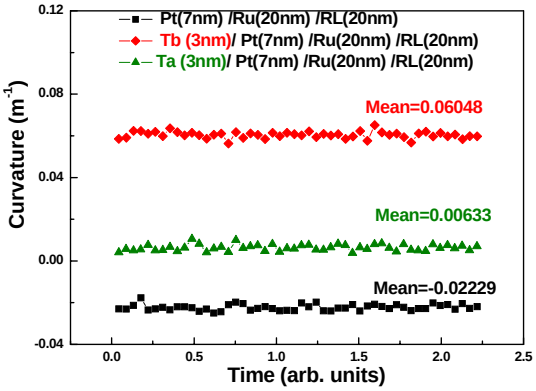

Figure 4.33 Curvature dependence of different media.

Table 4.1 Curvature and stress results of different media.

	Curvature (m^{-1})	Residual Stress
Si/Tb/Pt/Ru/CoPtCr-SiO_2	**0.06048**	**265.05 MPa (tensile)**
Si/Ta/Pt/Ru/CoPtCr-SiO_2	**0.00827**	**36.24 MPa (tensile)**
Si/Pt/Ru/CoPtCr-SiO_2	**0.02229**	**-97.68 MPa (compressive)**
Si/Tb	**0.03678**	**2.99 GPa (tensile)**
Si/Ta	**-0.01505**	**-1.16 GPa (compressive)**
Si	**-0.022**	

TABLE I
RESIDUAL STRESS INDUCED ON THE FILMS DURING THE SPUTTERING

Film structure (nm)	Residual Stress (MPa)
NiFeNb(200)	853
Ru(20)/Ta(5)/NiFeNb(200)	70
CoCrPtO(20)/Ru(20)/Ta(5)/NiFeNb(200)	480
CoZrNb(150)	-100
Ru(20)/Ta(5)/CoZrNb(150)	-450
CoCrPtO(20)/Ru(20)/Ta(5)/CoZrNb(150)	-311

Table 4.2 Residual stress induced on the films during the sputtering [25].

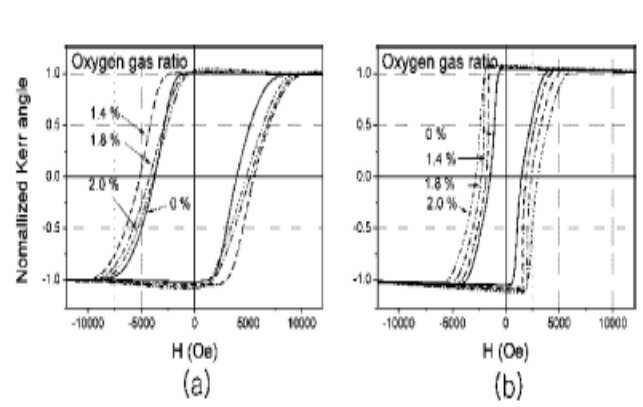

Figure 4.34 M-H loop of different media with (a)tensile stress and (b) compressive stress.[25]

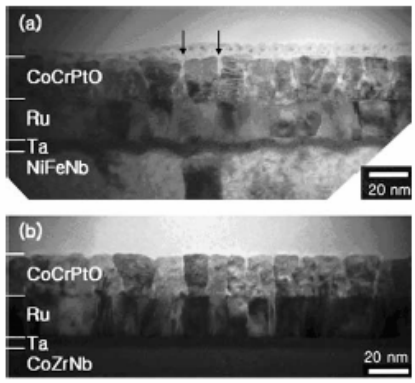

Figure 4.35 TEM cross-sectional images of different media with (a) tensile stress and (b) compressive stress [25].

In comparison with the reference paper [25], the magnitude of stress was similar to our result. Moreover, the larger tensile stress indeed played a vital role on the enhancement of magnetic properties as revealed in Fig. 4.34 and Fig. 4.35.

4.1.4.2 Microstructure observation

To further illustrate the stress effect of underlayers on the magnetic properties, plane-view TEM images and grain size distribution are shown in Fig. 4.36. It obviously indicates that the Tb buffer-layer significantly enhance the extent of SiO_2 segregation. Furthermore, the grain size of magnetic grains is also successfully reduced to 6nm due to the enhancement of SiO_2 segregation by introducing Tb buffer-layer. On the other hand, the grain size distribution of the media with Ta buffer-layer has narrowest distribution about 19.58 % and small grain size about 7.71nm. Consequently, the CoPtCr-SiO_2 media with Ta and Tb buffer-layer could both enhance the segregation and reduce grain size, which will narrow the c-axis distribution and enhance peak intensity

effectively, as well as the superior magnetic properties.

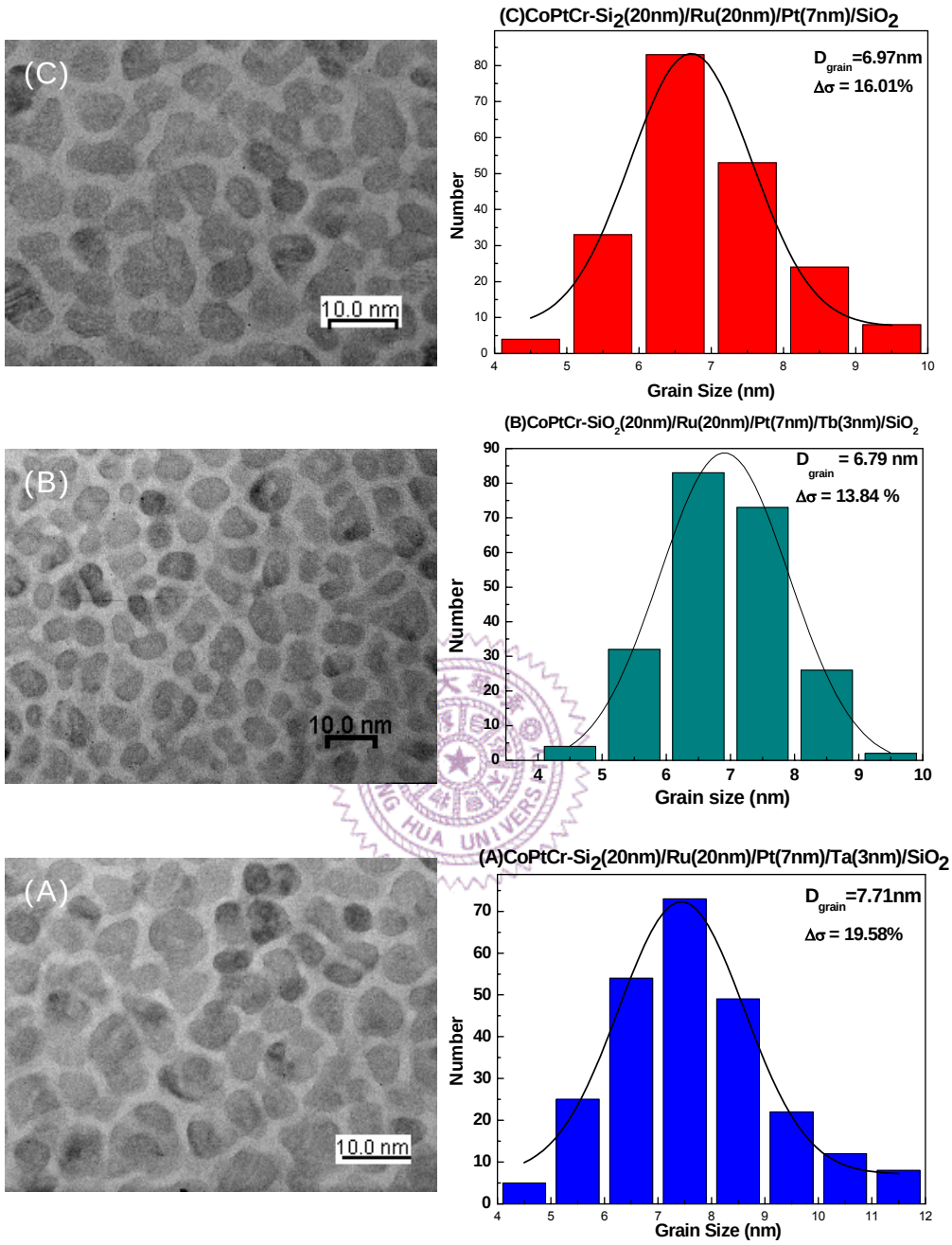

Figure 4.36 Plane-view TEM images and grain size distribution of these three media.

From the analysis of EDS, the compositions of grain and grain boundary are investigated as described in Fig. 2. The media B has most and less composition of (Si+O) at grain boundary and within the grain,

respectively. It implies that the degree of SiO_2 segregation of media B is higher than media A and C. The segregation enhancement may be attribute to the residual stress by depositing different underlayers.

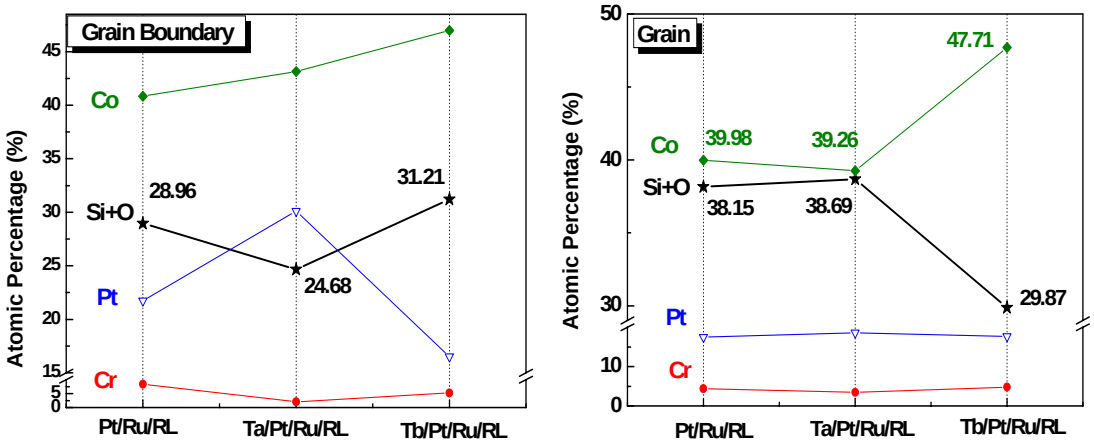

Figure 4.37 EDS analysis at grain boundary and within grain of these three media.

The effects of Tb/Pt/Ru underlayers on CoPtCr-SiO_2 perpendicular recording media shows not only the enhancement of magnetic properties but the microstructure observed from plane-view TEM images. It may conclude the change of in-plane residual stress from compressive to tensile stress that alter the degree of SiO_2 segregation and improve perpendicular and in-plane Hc in the same time.

Furthermore, the peak intensity of XRD profile and the FWHM value of c-axis distribution of the media with Tb/Pt/Ru underlayers are much superior to the media with Ta/Pt/Ru and Pt/Ru underlayers. In summary, the influence of Tb/Pt/Ru underlayer on magnetic properties and microstructure are extremely huge that we could apply this kind of underlayer on ultra-high recording density of perpendicular recording media in the future.

4.2 Effects of Working Pressure of Ru Seedlayer

4.2.1 Effect on Pt/Ru/CoPtCr-SiO_2 media

Increasing the working pressure of Ru seedlayer would attain lower out-of-plane lattice mismatch as shown in Fig. 4.38; however, the anisotropy orientation was destroyed as shown in Fig. 4.39 at the same time due to immensely raised in-plane Hc, though the perpendicular Hc was increased to almost 4000 Oe. In this case, deteriorated texture of recording layer would be usually accompanied with declined anisotropy orientation. In addition, the microstructure of the film as seen in Fig. 4.41 illustrated that the SiO_2 segregation at grain boundaries was enhanced as increasing working pressure which resulted in both reduction of grain size and narrowness of grain size distribution. Furthermore, the intergranular exchange coupling was significantly reduced due to improved segregation. As a result, the signal-to-noise ratio (SNR) of the perpendicular recording media would be promoted eventually.

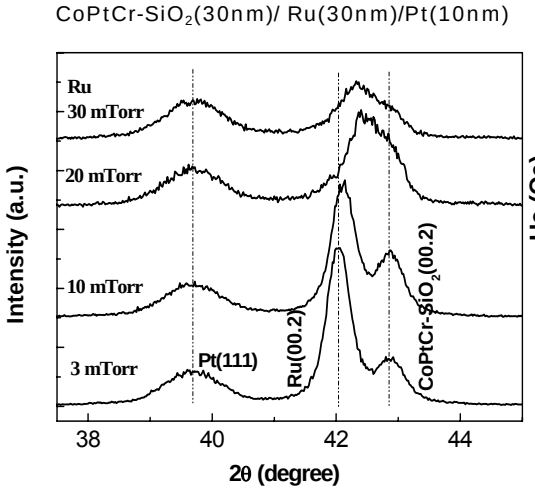

Figure 4.38 XRD profiles of working pressure effect on Ru seedlayer.

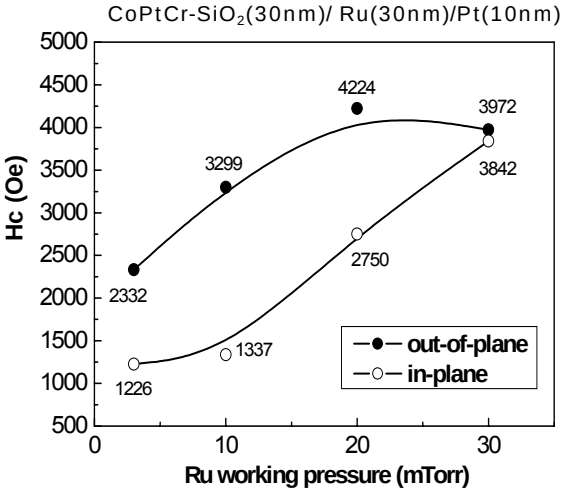

Figure 4.39 VSM results of working pressure effect on Ru seedlayer.

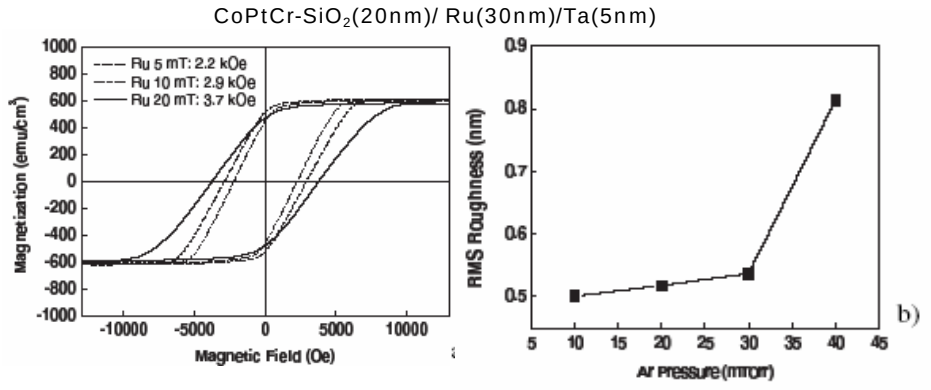

Figure 4.40 Dependences of Hc and roughness on working pressure of Ru seedlayer. [30]

Many researches had referred the enhancement of Hc to increasing roughness while increasing working pressure of Ru seedlayer, as reported in the study [30]. Fig 4.40 showed the evidence of the trend. In this thesis, enhanced perpendicular Hc was also accompanied with increasing working pressure. However, we would like to point out the stress effect may play an important role in the following discussion

From the cross-sectional TEM images as seen in Fig. 4.42, the large lattice mismatch at 3 mTorr of Ru seedlayer would tend to introduce an interfacial layer, while there was no interfacial layer at 20 mTorr of Ru seedlayer. The interfacial strain might also affect the interfacial composition and structure and the formation of interfacial layer might be related to the strain release, which resulted in good epitaxial growth. In addition, the segregation could be examined by EDX result as shown in Fig. 4.43, indicating that the increased working pressure of Ru seedlayer enhanced the grain boundary segregation and effectively eliminated the interfacial layer. Moreover, the grazing-incidence x-ray diffraction revealed that the lattice constants of the Ru layer decreased in both in-plane and out-of-plane directions when the working pressure of Ru was increased. Consequently, the lattice mismatch between Ru and the recording layer was reduced by increasing working pressure of the Ru

layer, as described in Fig. 4.44.

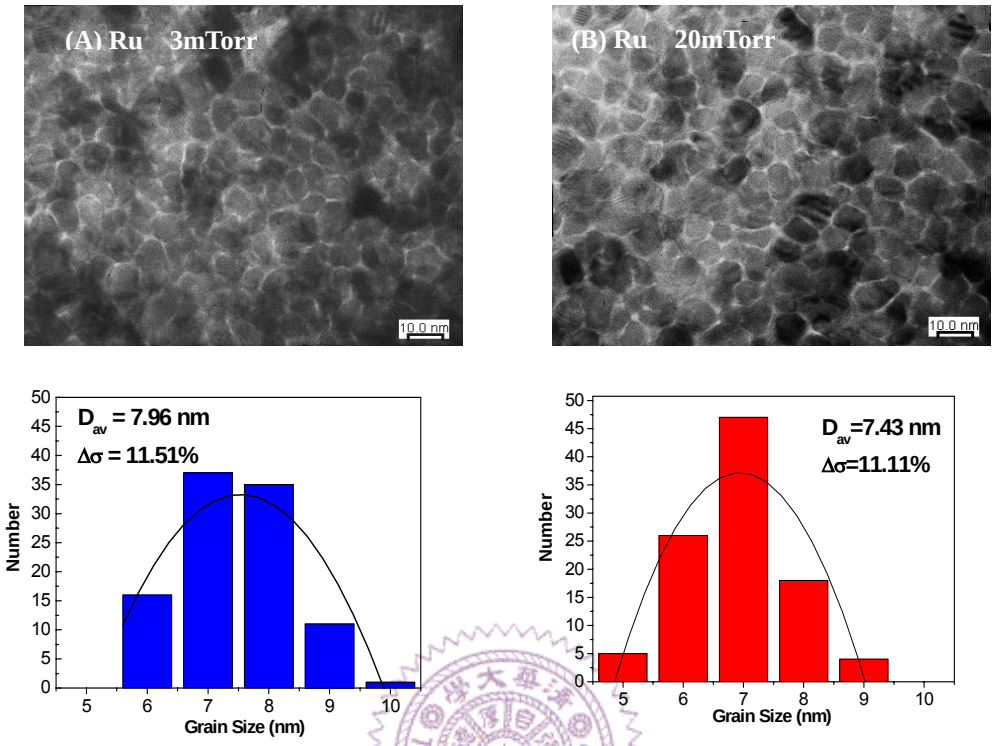

Figure 4.41 Plane-view TEM images and grain size distribution of working pressure effect on Ru seedlayer

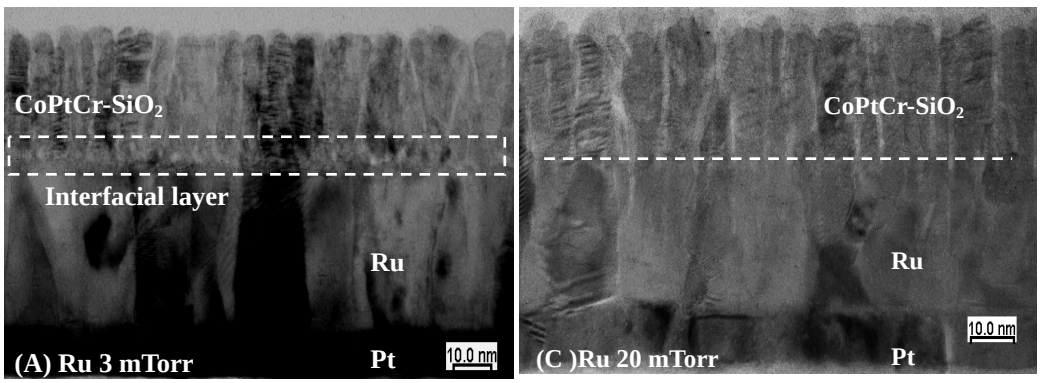

Figure 4.42 Cross-sectional TEM images of working pressure effect on Ru

Finally, the best working pressure of Ru seedlayer would be set at 20 mTorr in order to not only prevent declined anisotropy orientation but get relative good performance of segregation and c-axis orientation.

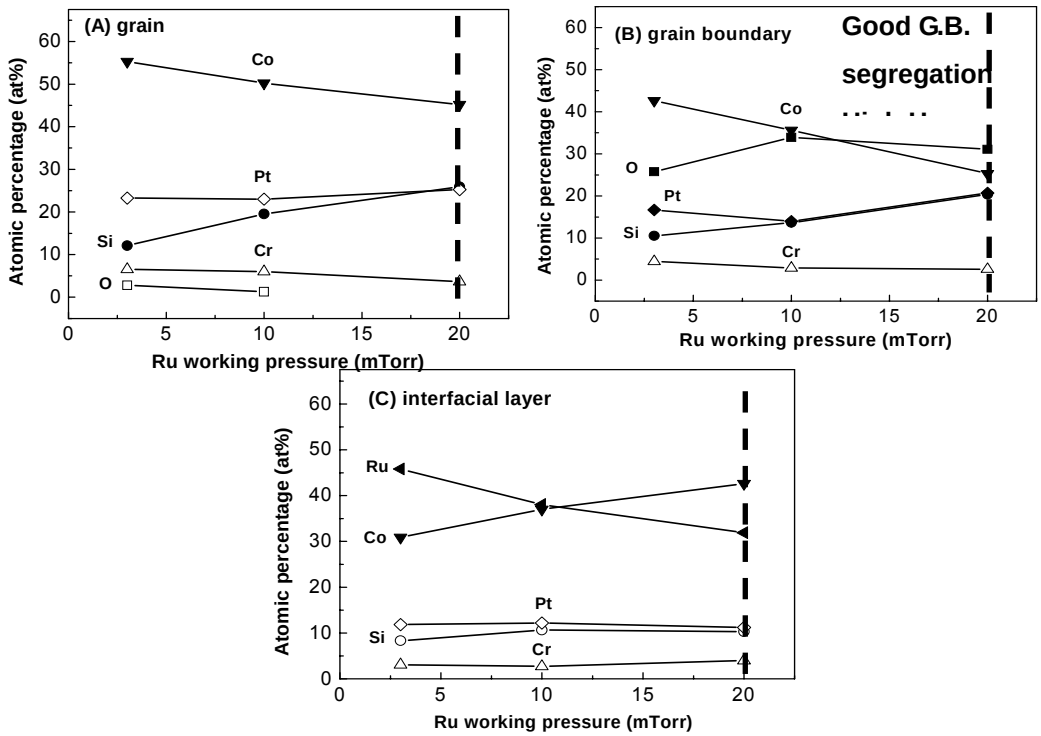

Figure 4.43 EDX result of working pressure effect on Ru seedlayer.

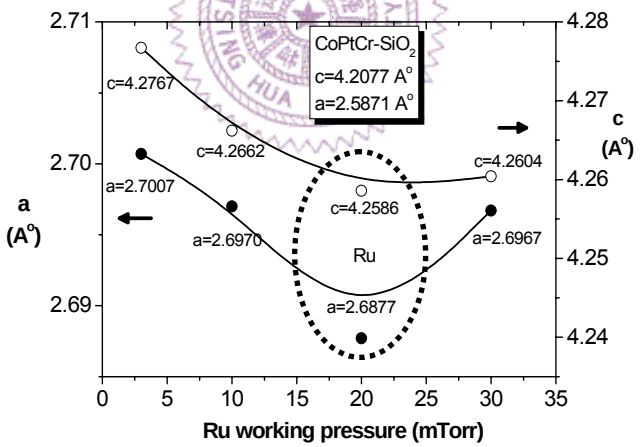

Figure 4.44 Lattice mismatch of working pressure effect on Ru seedlayer.

4.2.2 Stress Effect on Ta/Pt/Ru/CoPtCr-SiO_2 media

As just mentioned, increasing working pressure of Ru seedlayer is a controversial issue that many reports had indicated the importance of it.

We would re-examine the effect on the Ta/Pt/Ru/CoPtCr-SiO_2 media here. The perpendicular and in-plane coercivity both increased with working pressure of Ru (Fig. 4.45.). However, increasing Ru working pressure significantly broadens c-axis distribution ($\Delta\theta_{50}$) and results in increases in the in-plane Hc. Therefore, it is much clearer to compare the ratio of perpendicular coercivity to in-plane coercivity (Hc⊥/ Hc//) with c-axis distribution ($\Delta\theta_{50}$) as plotted in Fig. 4.46. As raising Ru working pressure, the ratio of coercivity tends to decrease while the c-axis distribution raises from 3.16 to 5.16. It indicates that the degraded structural orientation may deteriorate of magnetic properties due to increasing Ru working pressure.

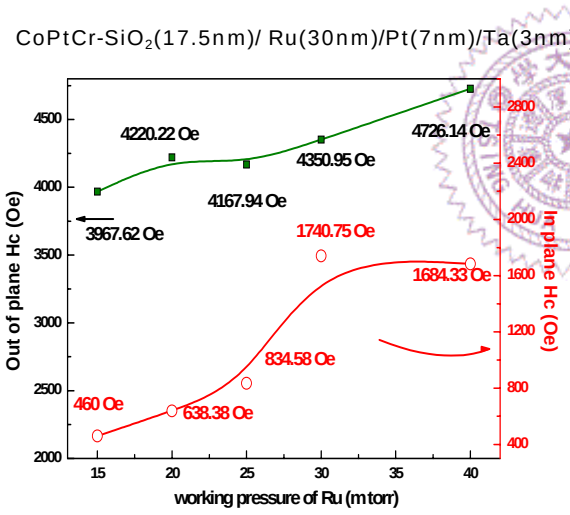

Figure 4.45 Coercivity dependence of working pressure of Ru seedlayer.

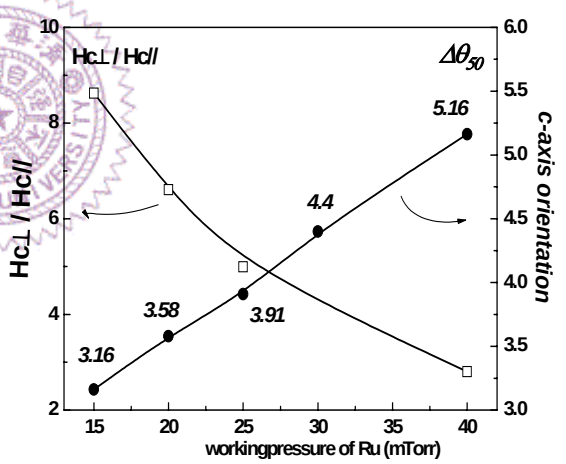

Figure 4.46 The dependence of c-axis distribution and anisotropy orientation of Ru working pressure.

From the XRD analysis of the Ta/Pt/Ru/CoPtCr-SiO_2 media with increasing Ru working pressure, the Ru(00.2) peak shifts to the high angles in x-ray diffraction patterns, as shown in Fig. 4.47. With increasing Ru working pressure from 5 mTorr to 40 mTorr, the peak of

Ru (00.2) tends to remove from low angle (42.10°) to high angle (42.50°). It represents that the film was under large in-plane tensile stress, which reduces c-lattice and increases a-lattice constant in the same time. The peak shift to high angle has also been evidenced from the result of bending-beam curvature measurement as shown in Fig. 4.48, where Stoney's equation is used for transferring curvature to stress. The in-plane residual stress of the film changes from -2.26 GPa (compressive stress) to 0.27 GPa (tensile stress) with increasing Ru working pressure, consistent with peak shift of Ru(00.2) in XRD. It successfully demonstrates the effect of Ru working pressure on crystallographic variation.

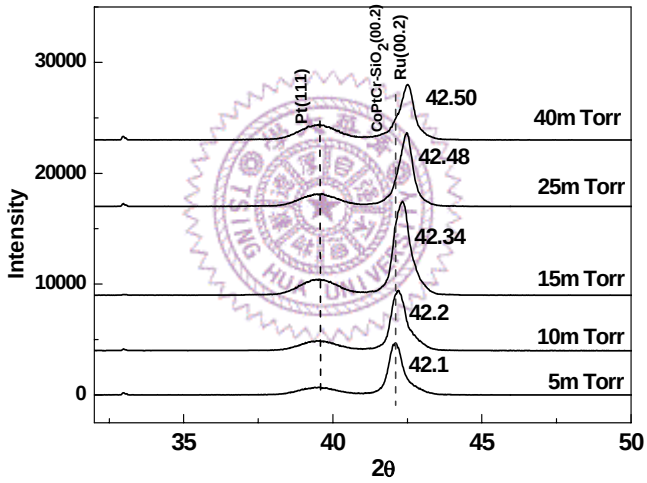

Figure 4.47 XRD profiles of increasing working pressure of Ru seedlayer.

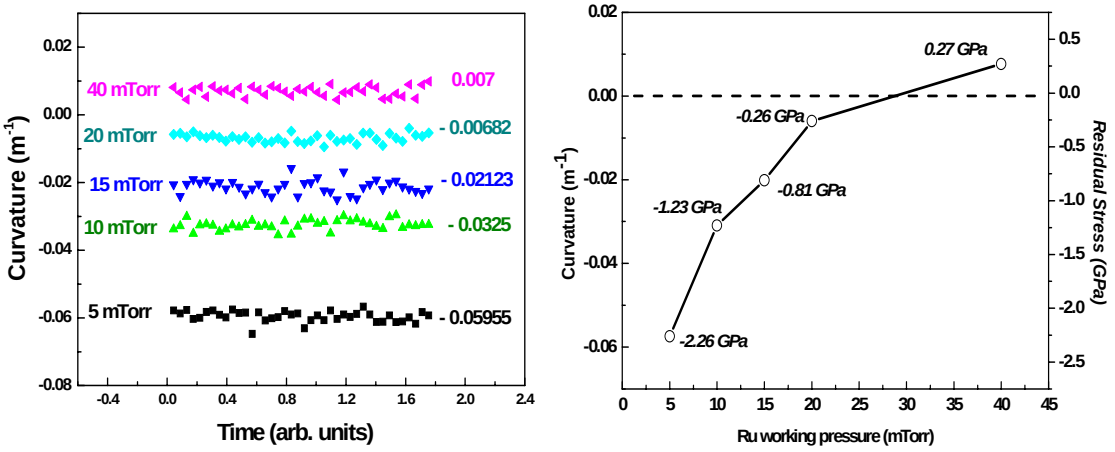

Figure 4.48 Curvature measurements of the films with increasing Ru working pressure.

$$\text{Stoney's Equation}: \quad \sigma = \frac{Es\,(t_S + t_F)^2}{6\,(1-\nu_S)\,t_F\,R}$$

Table 4.3 Curvature and stress dependence of increasing working pressure.

	5 mTorr	10 mTorr	15 mTorr	20 mTorr	40 mTorr
Curvature	**-0.05955**	**-0.0325**	**-0.02123**	**-0.00682**	**0.007**
Residual Stress	**- 2.26 GPa**	**- 1.23 GPa**	**-0.81 GPa**	**-0.26 GPa**	**+ 0.27 GPa**

In addition, the tensile stress may be associated with difference perpendicular Hc as shown in Fig. 4.45. The film with tensile stress shows larger perpendicular Hc about 4726.14 Oe while compressive one shows smaller Hc about 3967 Oe. It implies that the effect of Ru working pressure may also vary the magnetic properties of the film.

The increased intergranular exchange coupling tends to narrow the switching field distribution (SFD), i.e. the dispersion of the fields required to switch the magnetic clusters [39-41]. We introduce the relation of switching field distribution to increasing Ru working pressure as shown in Fig. 4.50, and 4.51. The standard deviation of switching field distribution is broadened as increasing Ru working pressure, which may correlate with the degraded c-axis distribution.

Many studies have shown the relation between the roughness and perpendicular Hc. The films without recording layer as Ta(3nm)/Pt(7nm)/ Ru(30nm) indicates that the roughness of the film is raised as increasing Ru working pressure (Fig. 4.52), the same as reported one [30].

Ru working pressure has many great effects on magnetic performance and crystallographic characteristics of the CoPtCr-SiO_2 media. Residual stress may be the main influence factor of the films with different

working pressure, which drives the Ru (00.2) peak from low angle to high angle. Although increasing Ru working pressure may enhance perpendicular Hc, it is accompanied with increased in-plane Hc, broadening c-axis distribution and switching field distribution. Finally, we present the same result of interfacial roughness as increasing Ru working pressure. Roughness at interface between Ru underlayer and recording layer may be an influence factor; however, the residual stress could give more information than roughness effect with respect to Ru working pressure.

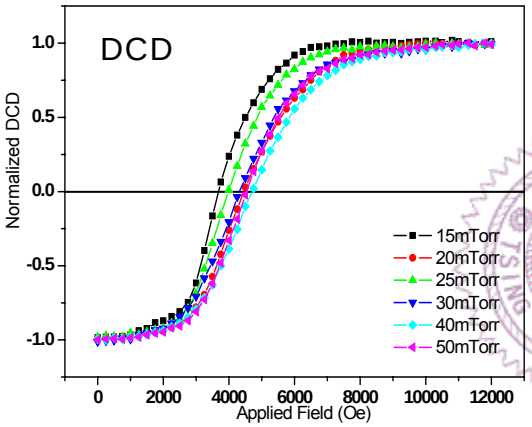

Figure 4.49 DCD curve of increasing Ru working pressure.

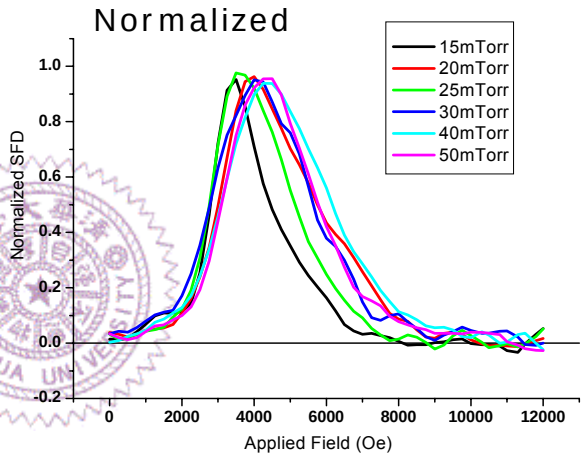

Figure 4.50 Normalized SFD profiles of increasing Ru working pressure.

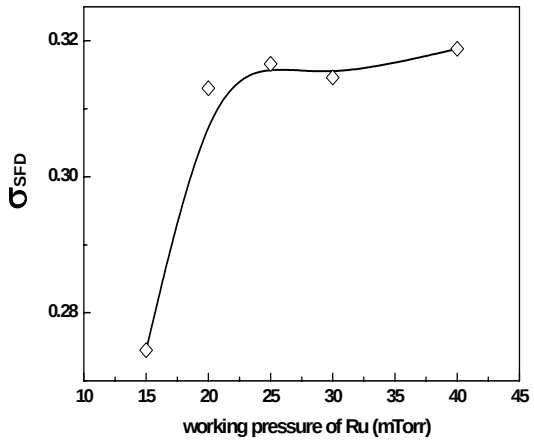

Figure 4.51 Standard deviation of SFD while increasing Ru working pressure.

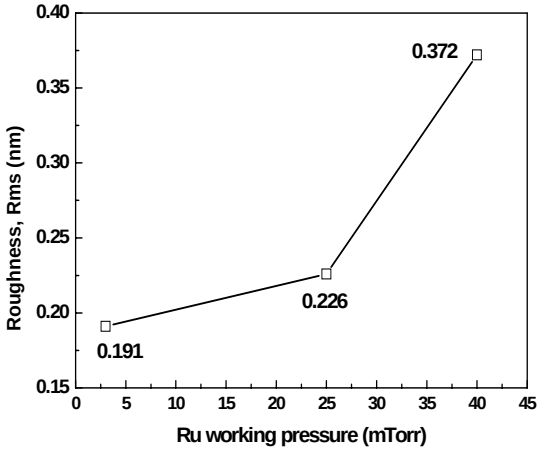

Figure 4.52 The morphology of roughness analyzed by AFM with respect to Ru working pressure.

4.3 Full-Stacked Structure

Since the recording system of Ta(3 nm)/Pt(7 nm)/Ru(30 nm)/CoPtCr-SiO2(17.5 nm) achieved the optimal properties of Hc~4.8 kOe, SQ~1, Hn~-2 kOe and mean grain size around 7.16 nm, the two kinds of soft underlayer system was prepared in the full-stacked structure for the R/W test eventually. These two candidates for soft underlayer were Ta(10 nm)/$NiFe_{20}$(5 nm)/$CoFe_{90}$(50 nm)/IrMn(8 nm)/**$CoFe_{90}$**(50 nm) and Ta(10 nm)/$NiFe_{20}$(5 nm)/$CoFe_{90}$(50 nm)/IrMn(8 nm)/**CoFeN**(50 nm).

In particular, it deserved to be mentioned that the remarkable guidance of the senior Ph. D. student of our lab, Ruo-Fan Jiang, had greatly contributed to the accomplishment of this study.

4.3.1 Media with Ta/$NiFe_{20}$/$CoFe_{90}$/IrMn/$CoFe_{90}$ Soft Underlayer

The medium of Al-Mg substrate/Ta(10nm)/$NiFe_{20}$(5nm)/$CoFe_{90}$(50nm)/IrMn(8nm)/$CoFe_{90}$(50nm)/Ta(3nm)/Pt(7nm)/Ru(30nm)/CoPtCr-SiO_2(17.5nm) showed perpendicular Hc from 4.7 kOe to 5.3 kOe, as seen in Fig. 4.53, which was due to the enhancement of the texture of CoPtCr-SiO2(00.2) as the result of Fig. 4.54. Furthermore, grain size and distribution of full-stacked structure were 6.756 nm and 13.93% respectively, which were even smaller and narrower than the recording system without soft underlayer as evidenced in Fig. 4.55 and Fig. 4.56. Moreover, the flattened surface of each layers were clearly shown in Fig. 4.57 due to our superior UHV-Sputtering System.

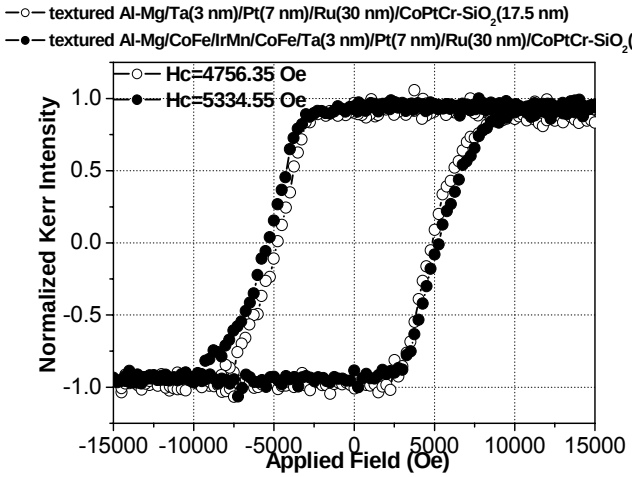

Figure 4.53 MH loops of these films with and without **CoFe** soft underlayer by PMOKE.

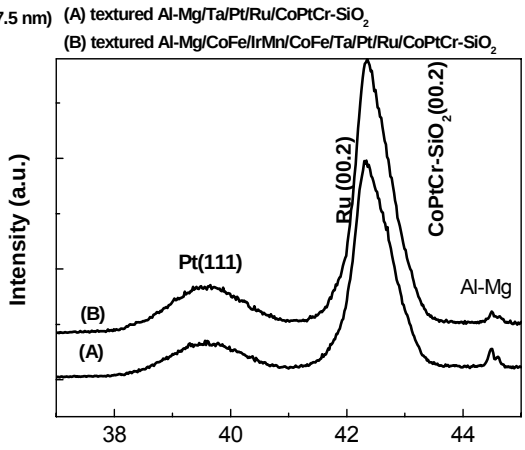

Figure 4.54 XRD profiles of these films with and without **CoFe** soft underlayer.

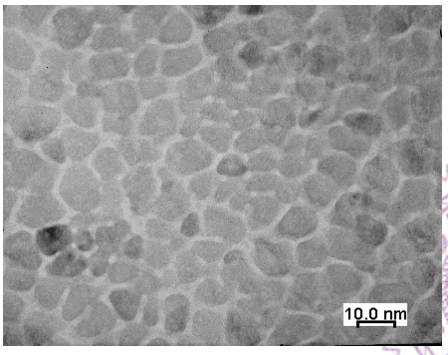

Figure 4.55 In-plane TEM image of Al-Mg substrate/Ta/$NiFe_{20}$/ $CoFe_{90}$/IrMn/ **$CoFe_{90}$**/Ta/Pt/Ru/ CoPtCr-SiO_2.

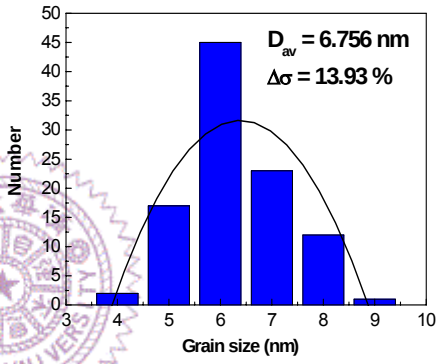

Figure 4.56 Grain size distribution of Al-Mg substrate/Ta/$NiFe_{20}$/ $CoFe_{90}$/IrMn/ **$CoFe_{90}$**/Ta/Pt/Ru/ CoPtCr-SiO_2.

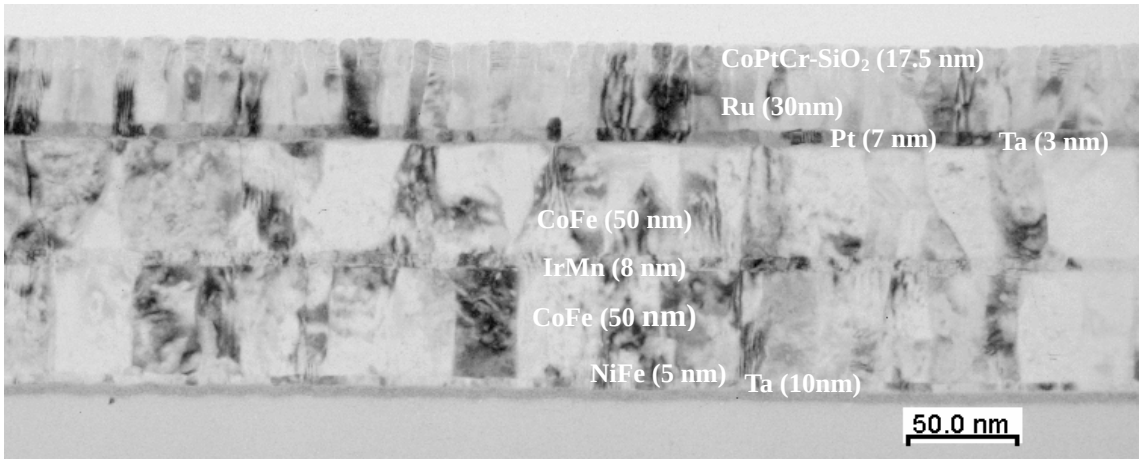

Figure 4.57 Cross-sectional TEM image of Al-Mg substrate/Ta(10nm)/$NiFe_{20}$(5nm)/ $CoFe_{90}$ (50nm) /IrMn(8nm)/**$CoFe_{90}$**(50nm)/Ta(3nm)/Pt(7nm)/Ru(40nm)/CoPtCr-SiO_2(17.5nm).

4.3.2 Media with Ta/$NiFe_{20}$/$CoFe_{90}$/IrMn/CoFeN Soft Underlayer

Although perpendicular Hc of this kind of CoFeN SUL was similar to CoFe SUL as plotted in Fig. 4.58, the texture of CoFe(110) had been destroyed as evidenced in Fig. 4.59. In spite of this, there was still a lot of space to optimize the texture of CoFe(110) while both the Ru(00.2) and CoPtCr-SiO_2(00.2) were greatly enhanced as adding the N_2 into the Ar when depositing. Trough the formation of CoFeN soft underlayer by adding N_2 into CoFe, it has superior soft magnetic properties to CoFe one and effectively promote the magnetic performance.

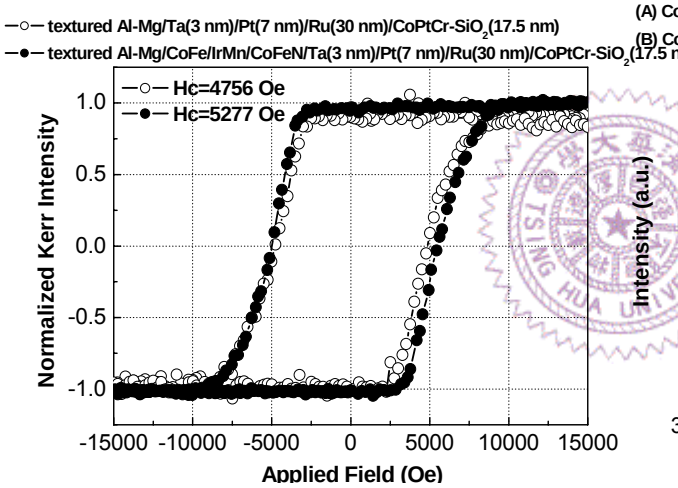

Figure 4.58 MH loops of these films with and without **CoFeN** soft underlayer PMOKE

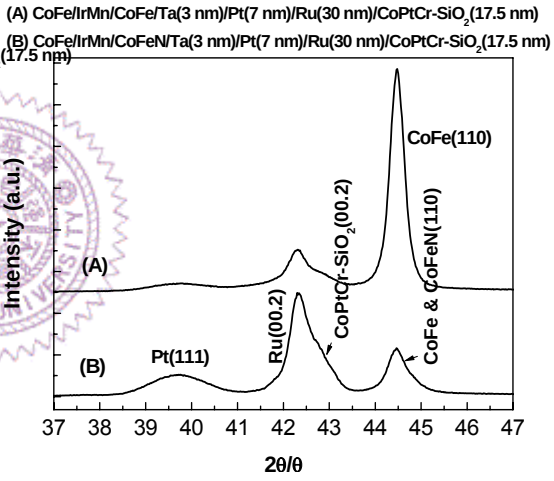

Figure 4.59 XRD profiles of these films with two different **CoFeN** soft underlayers

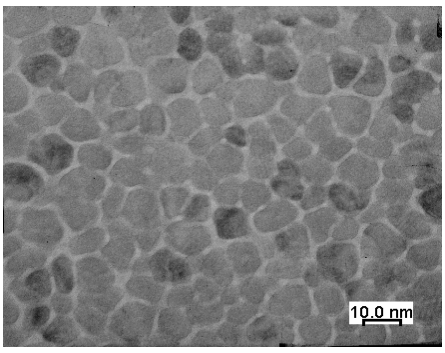

Figure 4.60 In-plane TEM image of Al-Mg substrate/Ta/$NiFe_{20}$/ $CoFe_{90}$/IrMn/ **$CoFe_{90}$N**/Ta/Pt/Ru/ CoPtCr-SiO_2

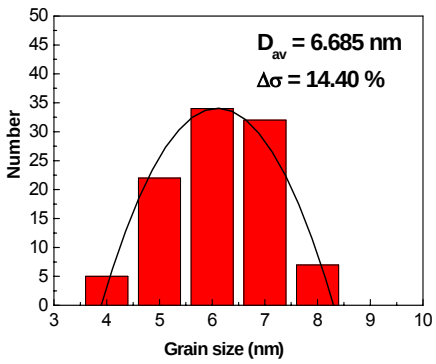

Figure 4.61 Grain size distribution of Al-Mg substrate/Ta/$NiFe_{20}$/ $CoFe_{90}$/IrMn/**$CoFe_{90}$N**/Ta /Pt/Ru/ CoPtCr-SiO_2

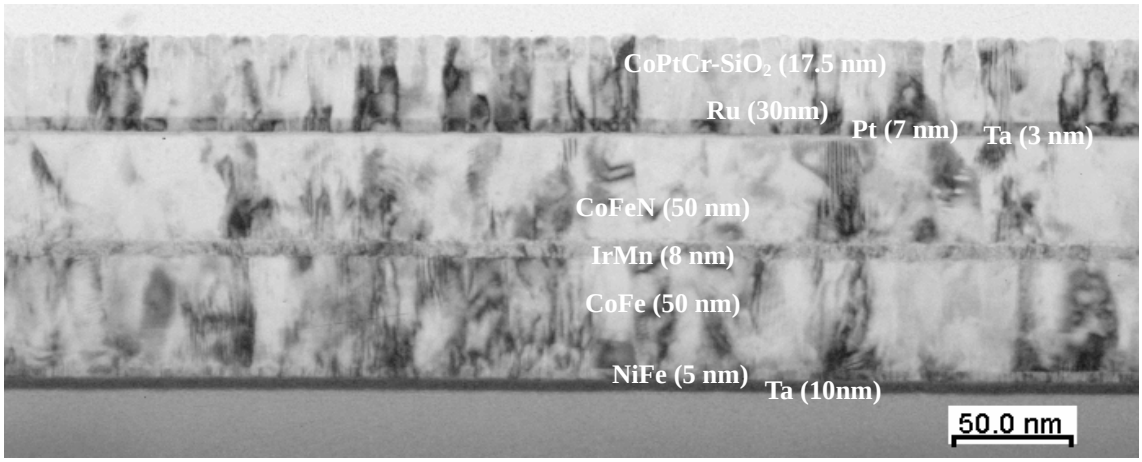

Figure 4.62 Cross-sectional TEM image of Al-Mg substrate/Ta(10nm)/$NiFe_{20}$(5nm)/ $CoFe_{90}$ (50nm) /IrMn(8nm)/**$CoFe_{90}N$**(50nm)/Ta(3nm)/Pt(7nm)/Ru(40nm)/CoPtCr-SiO_2(17.5nm)

Post-annealing

After full-stacked structure of the film was been established, post-annealing process was prepared to fix the magnetic moments of biasing layer/ soft underlayer by applying magnetic field about 1 kOe. As shown in Fig. 4.63 and Fig. 4.64, these full-stacked films after post-annealing were slightly promoted especially at magnetic performance measured by PMOKE measurement.

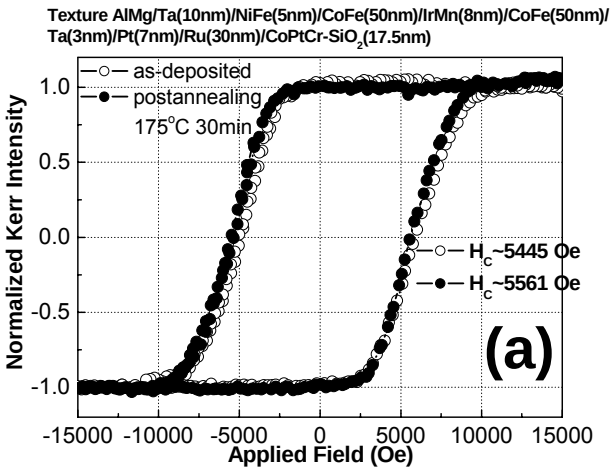

Figure 4.63 PMOKE results of as-deposited film and the one after post-annealing with **CoFe** soft underlayer

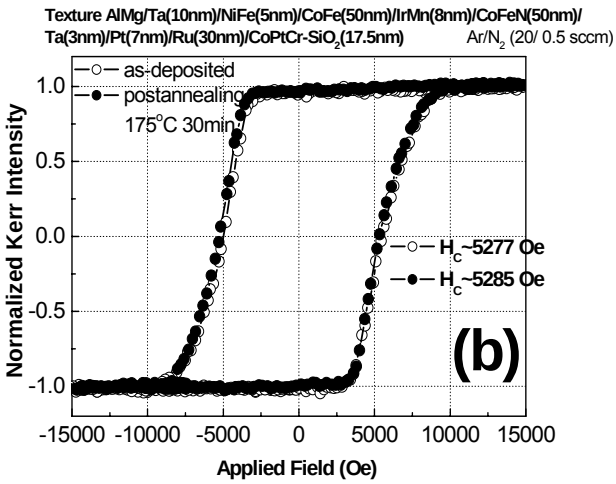

Figure 4.64 PMOKE results of as-deposited film and the one after post-annealing with **CoFeN** soft underlayer

4.3.3 R/W Test

4.3.3.1 PMR without SUL

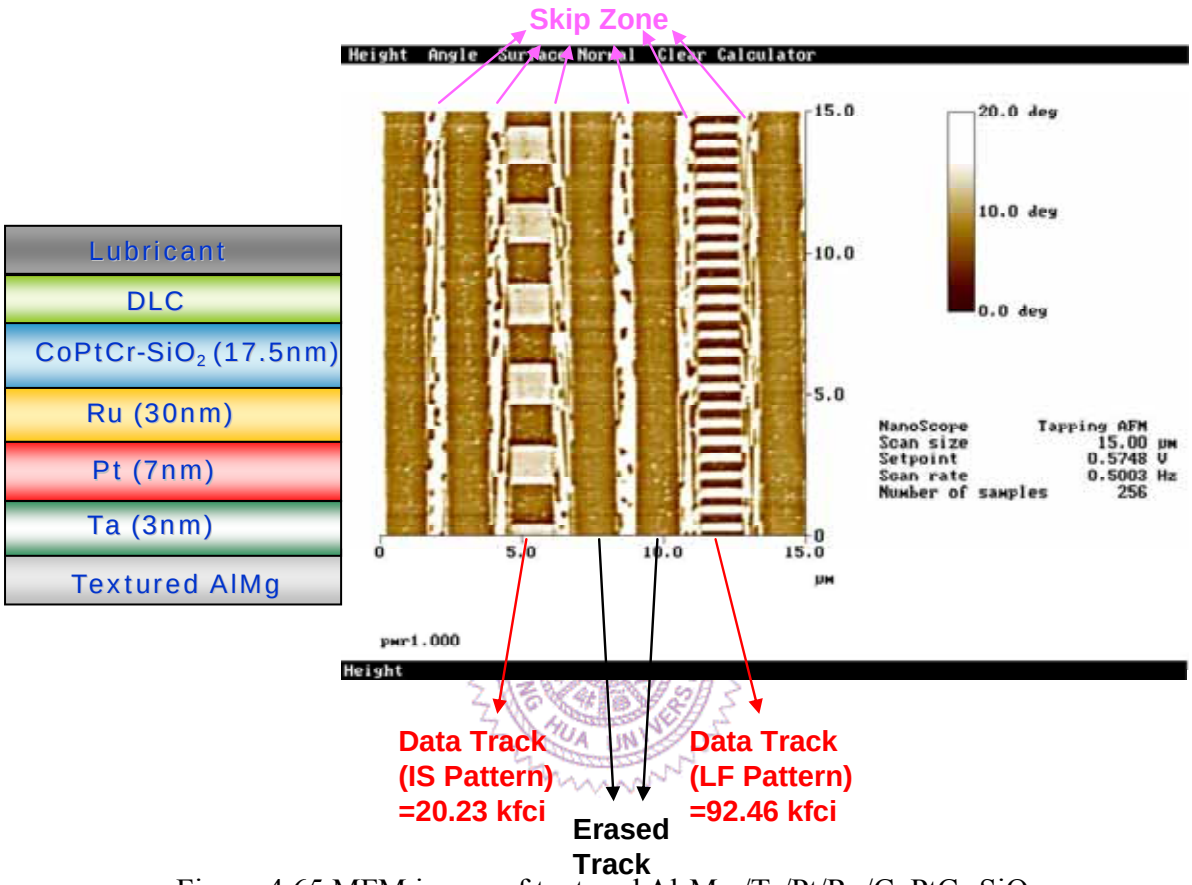

Figure 4.65 MFM image of textured Al-Mg /Ta/Pt/Ru/CoPtCr-SiO_2

As obviously indicated in Fig. 4.65, it implied that our structure was successfully developed for perpendicular recording media. Moreover, each clear data track of different recording density (20.23 kfci and 92.46 kfci) was recognized by using single-pole-type head (SPT head). The initial state of magnetic zone without R/W testing was shown in the region of "Skip Zone."

4.3.3.2 Full-Stacked PMR

Figure 4.66 MFM image of textured Al-Mg/Ta/NiFe/**CoFe**/IrMn/CoFe/Ta/Pt/Ru/CoPtCr-SiO_2

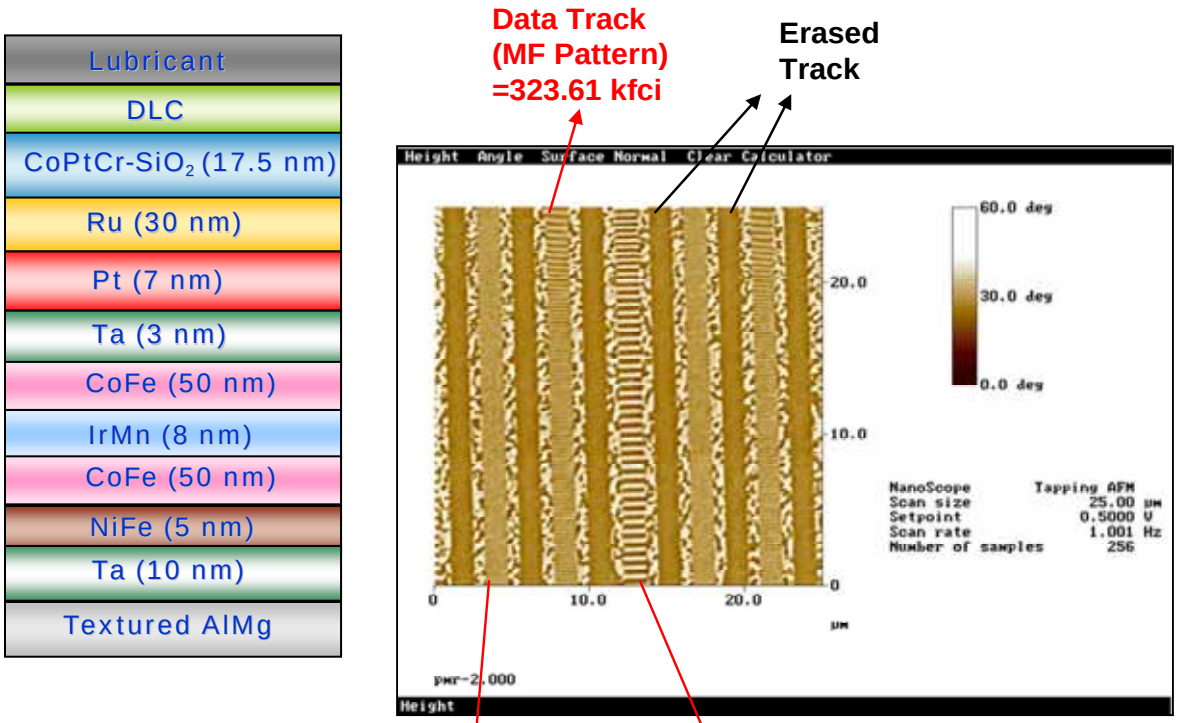

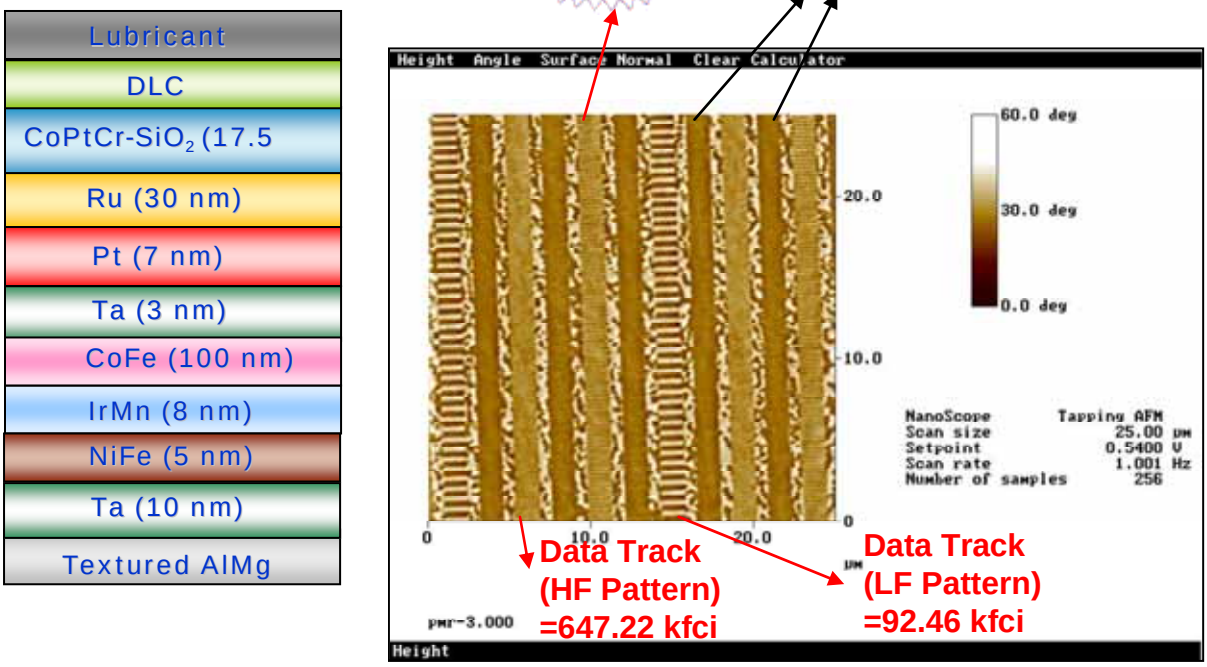

Figure 4.67 MFM image of textured Al-Mg/Ta/NiFe/IrMn/**CoFe**/Ta/Pt/Ru/CoPtCr-SiO_2

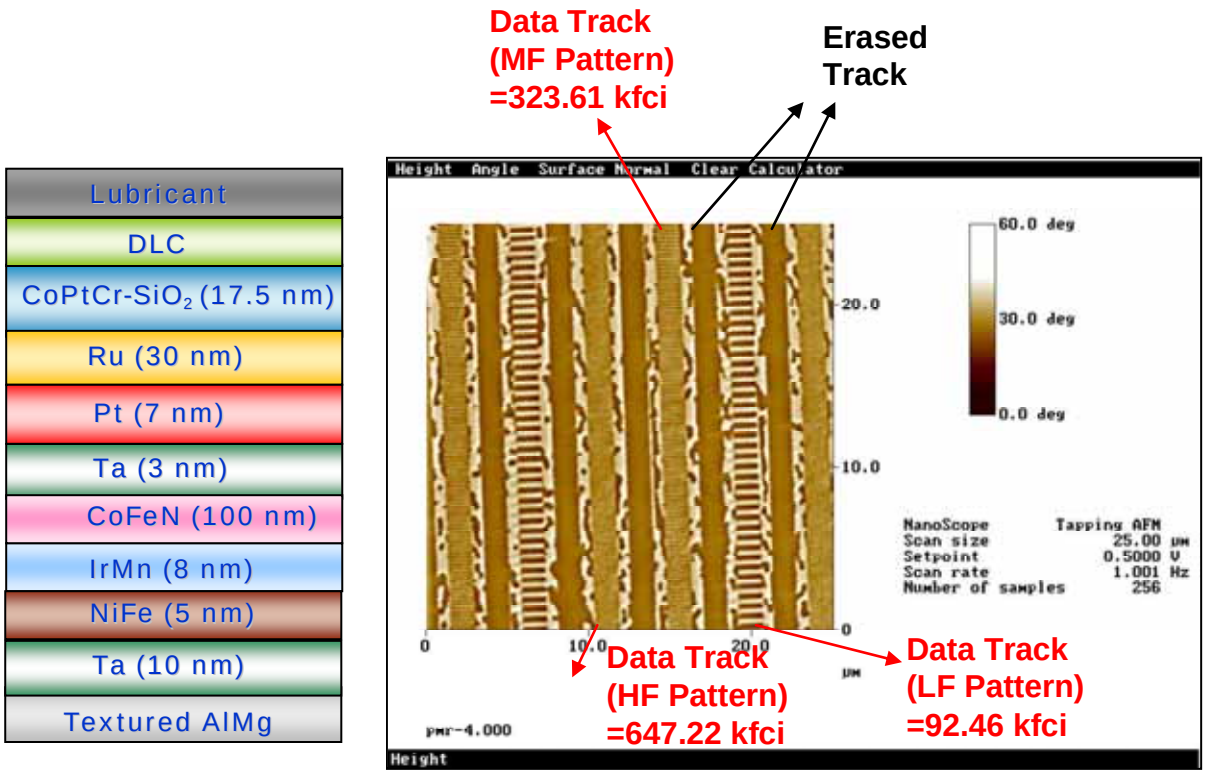

Figure 4.68 MFM image of textured Al-Mg/Ta/NiFe/IrMn/**CoFeN** /Ta/Pt/Ru/CoPtCr-SiO_2

In order to achieve the recording density beyond 100 Gb/in^2, the recording density of full-stacked media was examined by using a R/W tester with a SPT head. Concerning different recording density of ultra-high recording density media, writing the full-stacked media at the frequency from 92.46 kfci (low frequency-LF) to 647.22 kfci (high frequency-HF) was required. The data track of MFM images presented clear contrast between 1 and 0, which were observed in Fig 4.66, Fig. 4.67 and Fig. 4.68 at low frequency (92.46 kfci) and middle frequency (323.61 kfci); however, the data track at high frequency (647.22 kfci) presented indistinct readback signal. It might be due to insufficient small dimension of SPT head to extinguish the fine readback signal at high frequency.

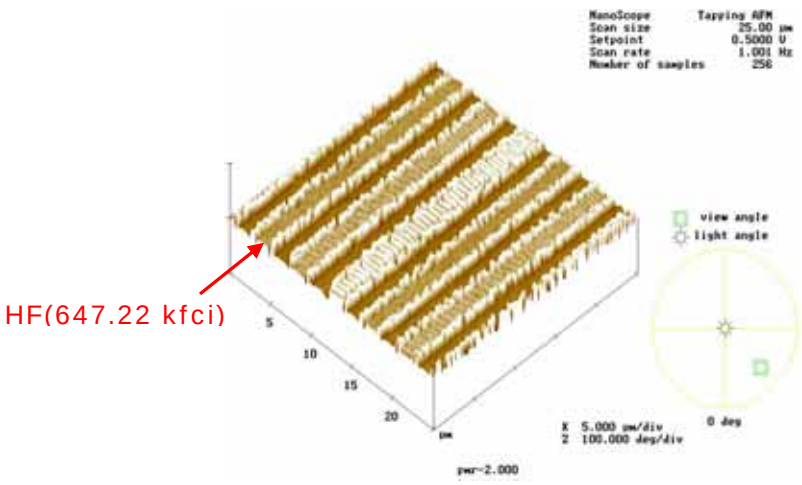

Figure 4.69 Cross-sectional MFM image Fig. 4.65.

Although the readback signal at high frequency was blurred, it was evidenced from cross-sectional MFM image as shown in Fig. 4.69 that the signal indeed existed at high frequency. In addition, the areal density of our media could be beyond 80 Gb/in^2 by calculating with respect to the linear density of readback signal at high frequency (647.22 kfci). It is expectable that our media have the most potential to achieve 100 Gb/in^2.

4.3.3.3 SNR result

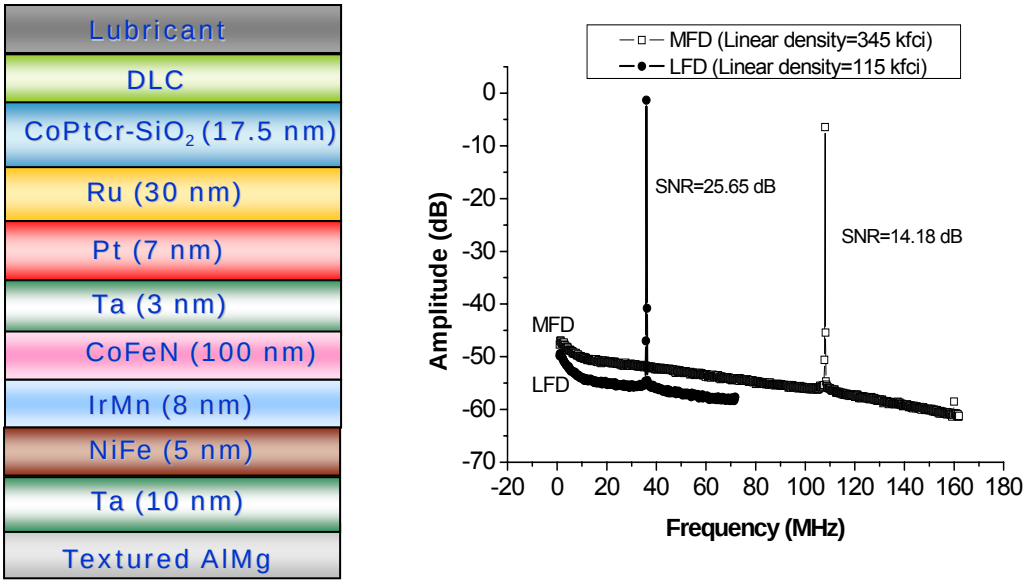

Figure 4.70 Linear recording density of full-stacked medium tested at different frequencies.

Fig. 4.70 shows the SNR performance of R/W test, investigated by a STP head at different frequencies. Low frequency (LF) and medium frequency (MF) were 115 kfci and 345 kfci, respectively. The SNR result of the medium tested at low frequency was 25.65 dB while the one at medium frequency was still 14.18 dB.

In comparison our result with the data reported in 2003 [46] as observed from Fig. 4.71, the SNR performance of ours was similar to the reported one though the thickness of our recording media was thicker than the reported one. It represents that our films own the most potential to get better recording performance than others in the future and can be extended to the recording density beyond 100 Gb/in^2.

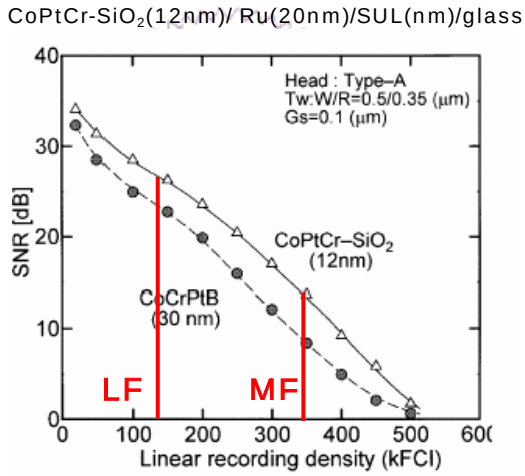

Figure 4.71 Recording density dependence of SNR for different media [46].

4.4 100 Gb/in^2 PMR

In order to make the result of R/W test be more convinced, it was indispensable to compare our result with the performance of 100 Gb/in^2, which is announced by Seagate global storage research centers. It was apparently recognized from Table 4.4 as illustrated below that not only perpendicular Hc and Ms were enhanced but grain size and distribution were extremely reduced through our remarkable efforts. In conclusion, our media is undoubted best and the most convinced film structure to achieve 100 Gb/in^2.

Organization	**Seagate(2002)-100Gb/in^2**	**NTHU-MSE**
RL (nm)	11nm	**17.5nm**
IL (nm)	4nm	**40nm**
SUL (nm)	200nm	**105nm**
Hc (Oe)	5000 Oe	**5561 Oe**
Ms (emu/cc)	380 emu/cc	**450 emu/cc**
Grain size (nm)	～9nm	**～6nm**
Dev. of grain size	0.25	**0.139**

Table 4.4 Compare our optimal performance with the simulation result announced by Seagate Storage Center in 2002.